A STUDY OF ELECTROMAGNETIC INDUCTION SYSTEMS FOR THE DETECTION OF UNEXPLODED ORDNANCE

Except where reference is made to the work of others, the work described in this thesis is my own or was done in collaboration with my advisory committee. This thesis does not include proprietary or classified information.

Neha Jain

Certificate of Approval:

Stuart Wentworth Associate Professor Electrical and Computer Engineering	Lloyd S. Riggs, Chair Professor Electrical and Computer Engineering
Ramesh Ramadoss Assistant Professor Electrical and Computer Engineering	George T. Flowers Interim Dean Graduate School

A STUDY OF ELECTROMAGNETIC INDUCTION SYSTEMS FOR THE DETECTION OF UNEXPLODED ORDNANCE

Neha Jain

A Thesis

Submitted to

the Graduate Faculty of

Auburn University

in Partial Fulfillment of the

Requirements for the

Degree of

Master of Science

Auburn, Alabama
May 10, 2008

A STUDY OF ELECTROMAGNETIC INDUCTION SYSTEMS FOR THE DETECTION OF UNEXPLODED ORDNANCE

Neha Jain

Signature of Author

Date of Graduation

THESIS ABSTRACT

A STUDY OF ELECTROMAGNETIC INDUCTION SYSTEMS FOR THE DETECTION OF UNEXPLODED ORDNANCE

Neha Jain

Master of Science, May 10, 2008
(B. E., Chhotu Ram State College of Engineering, MDU University, 2004)

83 Typed Pages

Directed by Lloyd S. Riggs

This thesis presents a study of a time domain electromagnetic induction (EMI) system used for detection and discrimination of unexploded ordnance. In general, EMI system components include transmitter and receiver coils, corresponding transmitter and receiver coil amplifiers and a data acquisition system. This thesis explains differences in electronic circuitry of EMI sensors that measure the current or voltage response of a target. In the case of a current measurement it is essential to use a current-to-voltage converter as the first stage before any amplification is done so that the lower 3 dB point of the receiver coil is sufficiently low to capture all important target characteristics. Also using a compensation circuit to lower the 3 dB point makes it possible to acquire the undistorted late time response of targets. This capability is essential for discrimination purposes. In voltage measurement methods, however, only a voltage amplifier is used on

the receiver side and there is no need for compensation circuitry as the 3 dB point of the receiver coil is high enough to capture an undistorted version of the target response. Both voltage and current measurement methods were used to record the target response and it was observed that in general, the voltage measurement method is better than the current measurement method. Comparison of the response collected from a commercial EMI sensor and a constructed EMI sensor (voltage method) is made. Observations are made for possible reasons for superior response from the commercial EMI sensor

In addition to the above topics, a software tool is developed for evaluating electromagnetic transmitter coil designs and configurations that are used in EMI sensor arrays. This software tool generates static sensitivity maps in any desired plane when transmitter and receiver coil space coordinates are given as inputs. These maps give a good idea of how effective an EMI sensor layout can be in terms of its sensitivity to a target's presence at different points in space. The advantage of using static sensitivity maps is that they are independent of target characteristics and thus can be used as an effective tool to measure the performance of a proposed coil layout. Maps have been presented for different coil configurations and important observations and conclusions are made. To verify the fidelity of the software tool output field measurements are taken using a commercial sensor and compared to the same from the software model. In general, good qualitative agreement was obtained though more careful measurements should be done in the future. In addition to sensitivity maps, streamline plots can also be generated from a similar software tool with minor changes in software coding. Streamline plots are helpful in visualizing the direction of the magnetic field due to transmitter or receiver coils in any orientation.

ACKNOWLEDGEMENTS

I would like to express my gratitude to Dr. Lloyd S. Riggs, my advisor, for providing technical direction, support and guidance during the course of this research. I would like to thank Dr. Stuart Wentworth and Dr. Ramesh Ramadoss for agreeing to serve on my thesis committee. My research team members Sailaja, Jithendra also deserve my appreciation for their support.

I would like to thank my mother, Kamini Jain for her enduring love, and moral support throughout my life. Finally, my husband, Varun Mahajan deserves credit for his constant encouragement, patience, and sacrifice.

Style manual of journal used: Graduate School: Guide to preparation and submission of theses and dissertations

Computer software used: Microsoft Office 2003, Vista

TABLE OF CONTENTS

LIST OF FIGURES

CHAPTER 1

INTRODUCTION

Unexploded ordnance (or UXO) are explosive weapons (bombs, shells, landmines etc.) that remain undetonated due to some malfunction when they were employed and therefore pose a severe danger of detonation potentially many decades later after they were used or discarded. In addition to this they also pose danger of environmental contamination as harmful chemicals like explosives can enter underground soil and water.

There have been countless cases of civilians tampering with unexploded ordnances that are many years old, often causing fatalities [1]. Landmine Monitor report identified at least 7,328 new landmine/ERW (explosive remnants of war) casualties in calendar year 2005—721 (11 percent) more than in 2004 (6,607). It is important to remember, however, that the 7,328 figure represents only the reported casualties and does not take into account many casualties that are believed to go unreported; in some countries, civilians are killed or injured in remote areas away from any form of assistance or means of communication; in some countries, casualties are not reported for military or political reasons. While acknowledging that it is not possible to know with absolute certainty, Landmine Monitor continues to estimate that there are between 15,000 and 20,000 new landmine/ERW casualties each year. The vast majority

(81 percent) of new landmine casualties in 2005 were civilians, as in past years. The 2005 total included at least 1,518 children (21 percent) and 347 women (5 percent). Nineteen percent of the reported casualties were identified as military personnel (1,404), a decrease from 25 percent (1,650) in 2004 [2].

The need of eradicating the UXOs and saving limbs and lives in every region of the world makes it important to improve the methods to detect them. EMI sensors and magnetometers are some of the several technologies that are being used to detect and discriminate UXO. However, the classification and discrimination of the detected anomalies still remains a significant challenge. Discrimination of UXOs is important to reduce the false alarm rates from metallic clutter and uninteresting objects such as shrapnel, bullet slugs and casings, nuts and bolts, etc. Also, there is significant data variability due to variable depths and orientations of even the known UXO targets [3].

This thesis addresses the key issues related to enhancing the discrimination capability of the EMI sensor and is an extension of previous work done at Auburn University and elsewhere in increasing EMI sensor potential in detecting and discriminating UXOs [4], [5]. It presents an effort towards the development of a time domain EMI sensor to give an accurate representation of target (UXO) response function. In addition to this it also explains the static sensitivity maps that characterize the EMI sensor layout without involving target features and without actually building the sensor and hence easing their design process. The maps are generated using a software tool which was built using MATLAB[1] (2006). This work was sponsored by US Army Corps of Engineers (Huntsville, Al).

This research contains six parts: Chapter 2 provides a brief introduction and description of EMI sensors in general. Chapter 3 discusses the two measurement methods, voltage and current, for obtaining the response from a time domain EMI sensor. Chapters 4 and 5 present an overview of the hardware which was constructed as a part of this effort and a comparison of data collected with the constructed EMI system to the same from a commercial EMI system (the EM63 sensor manufactured by Geonics Ltd.) [12] is also provided. Chapter 6 presents static sensitivity maps for evaluating coil designs and configurations used in the geophysical detection of UXO. Appendix A gives the details of the software tool designed to produce sensitivity maps.

Finally Chapter 7 summarizes research accomplishments and offers suggestions for future work research efforts.

---

[1] MATLAB is a registered trademark of The MathWorks, Inc. For MATLAB product information, please contact The MathWorks, Inc., 3 Apple Hill Drive, Natick, MA 01760-2098, Tel: (508) 647-7000, Fax: (508) 647-7101.

CHAPTER 2

BASICS OF ELECTROMAGNETIC INDUCTION SENSOR

In this chapter the basic principle and configuration of time domain electromagnetic induction sensors [6], [7] is discussed.

2.1 Introduction to EMI sensors

An EMI sensor usually consists of transmitter and receiver coils which are used to detect the presence of metallic objects underneath the earth's surface. In a pulsed or time domain EMI system, pulses of current are passed through the transmitter coil (we used a repetition rate of 50 Hz). This generates a time varying primary magnetic field in the surrounding environment which induces eddy currents in the buried conducting target [8]. Target eddy currents generate a secondary time-changing magnetic field. This secondary magnetic field induces a voltage in the receiver coil that can be amplified and used to detect and discriminate among UXOs. The primary magnetic field of the transmitter coil also reacts with the receiver coil and induces a direct coupled voltage in it. Thus the receiver voltage consists of two components: direct coupled voltage from the transmitter coil and secondary voltage due to object eddy currents. The unwanted direct coupled voltage component can be minimized by using a bucking or *figure 8* coil configuration in which each loop of the figure eight coil couples equally but oppositely to the transmitter coil thus zeroing the direct coupled voltage component. Figure 2.1 shows typical components of an EMI system.

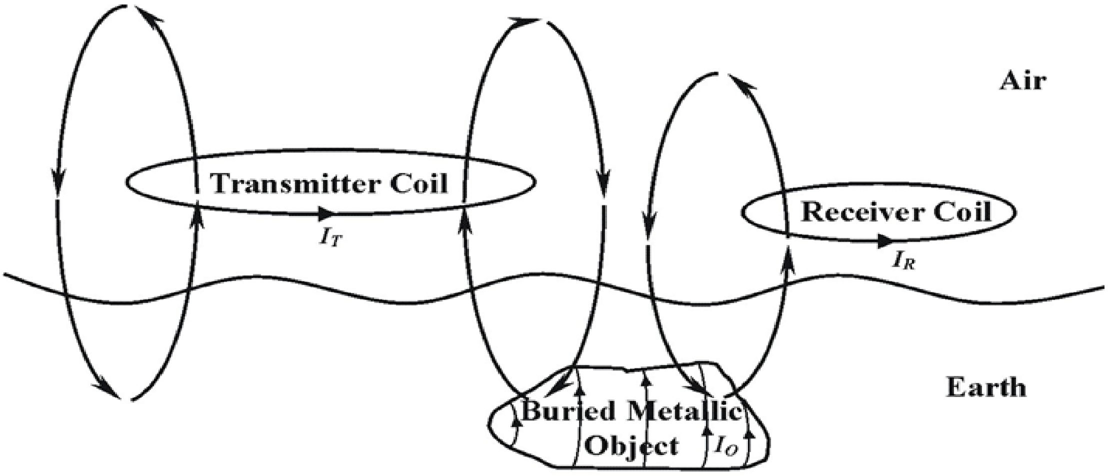

Figure 2.1 Typical electromagnetic induction system consisting of transmitter and receiver coil, shown here in the presence of a buried metallic object.

2.2 Simple Circuit Model of a Pulsed EMI system

In a time domain EMI system the transmitter coil is excited with current pulses of short duration that rise to a maximum value, stay at that value for some time, and then abruptly fall to zero in an exponential or linear (preferred) fashion. A shunt resistance across the transmitter coil reduces ringing or oscillations produced due to second order interaction between the coil inductance and parasitic capacitance [5]. The value of this shunt resistor can be adjusted by observing the transmitter current waveform on an oscilloscope. If the value of Rshunt is very low compared to the parasitic capacitance it will make the turn off occur slowly (over damped system) and if it is very high it will lead to ringing (under damped system). Therefore the shunt resistance should be adjusted in such a way that the response is critically damped. Figure 2.2 shows a simple coil model that includes parasitic coil capacitance. Figure 2.3 shows the effect of different Rshunt values on the current waveform when the dc supply is suddenly removed (using a switch). Parasitic coil capacitance is assumed very large (in microfarads) in this model for clear display purposes only.

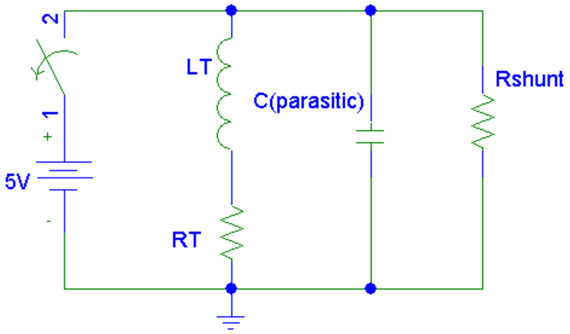

Figure 2.2 Simple Transmitter Coil Model including parasitic capacitance effects and Rshunt that is used to reduce ringing during turn off of transmitter current.

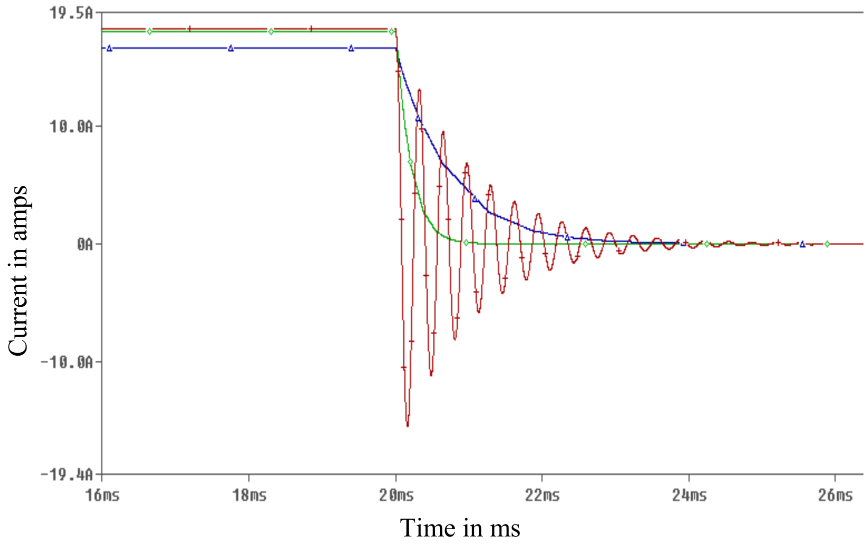

Figure 2.3 Current Waveforms through the transmitter coil when the closed switch was suddenly opened at 20ms. Red curve is for very high value of Rshunt, green is for low value of Rshunt and blue curve is for very low value of Rshunt.

Shown in Figure 2.4 is a magnetically coupled circuit model of an EMI sensor (Time Domain or Continuous Wave). The Continuous Wave (CW) sensor uses a discrete number of sinusoidal signals to excite the transmitter coil instead of pulses that are used in Time Domain (TD) sensors [8]. The transmit coil is assumed to have self inductance and resistance, L_T and R_T, respectively. Similarly, the object and the receiver coil can be represented by an inductance L_O, L_R and resistance R_O, R_R, respectively. This representation of the object is accurate only for a simple first order object such as a loop of thin copper wire (radius of the wire much less than the radius of the loop), and does not hold for more complex objects like the sphere or cylinder. Also, the input impedance of the receiver amplifier is represented as Z_R and the transmitter, object, and receiver currents are given as I_T, I_O and I_R, respectively. The mutual coupling between the transmitter and the object, object and the receiver coil, and the transmitter and the receiver are denoted as M_{TO}, M_{OR}, and M_{TR}, respectively. The mutual coupling M_{TR} induces a voltage V_{DIRECT} (generally undesirable) in the receiver coil [4].

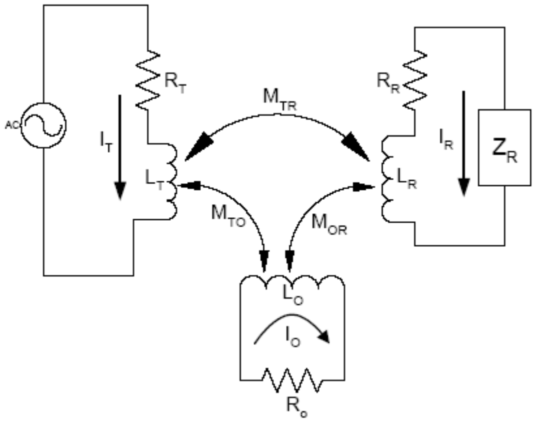

Figure 2.4 Magnetic Coupled Circuit representing a TD / CW EMI sensor [4].

2.2.1 Object Current

According to Faraday's law of induction [9] the voltage induced in the object is the product of mutual coupling between object and transmitter coil and the time rate of change of transmitter current, i.e.

$$V_{OBJECT} = -M_{TO} \frac{dI_T}{dt} \tag{2.1}$$

According to Figure 2.5 the transmitter current is constant at I_I for times t<0, and for time $0 \leq t \leq T$ the current decays linearly to zero at t = T assuming an ideal case. Thus the voltage induced in the object is zero for time t<0. As shown in Figure 2.6 when the switch is in position A, the transmitter current decays linearly (0≤t≤T), and the voltage induced in the object is constant and is equal to $M_{TO}I_I/T$. During this period, the object eddy currents exponentially build up as shown in Figure 2.7(b).

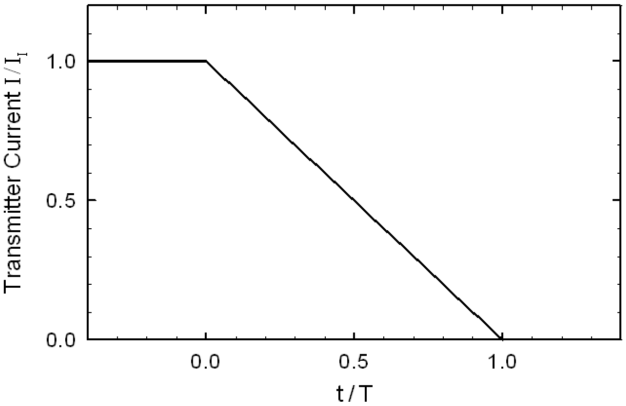

Figure 2.5 Normalized transmitter current versus normalized time.

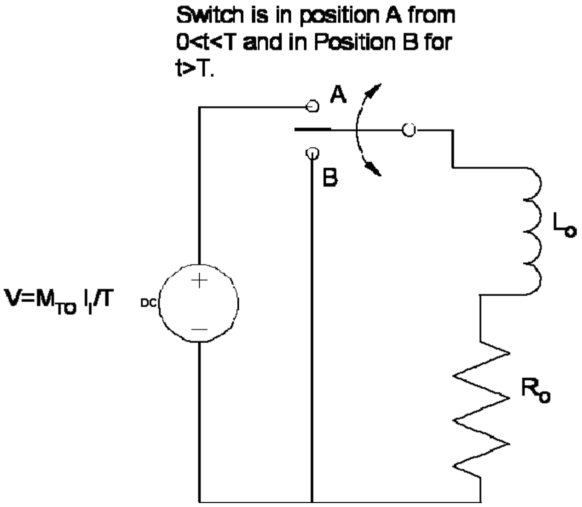

Figure.2.6 Circuit model of object explaining the charge up and decay of object currents.

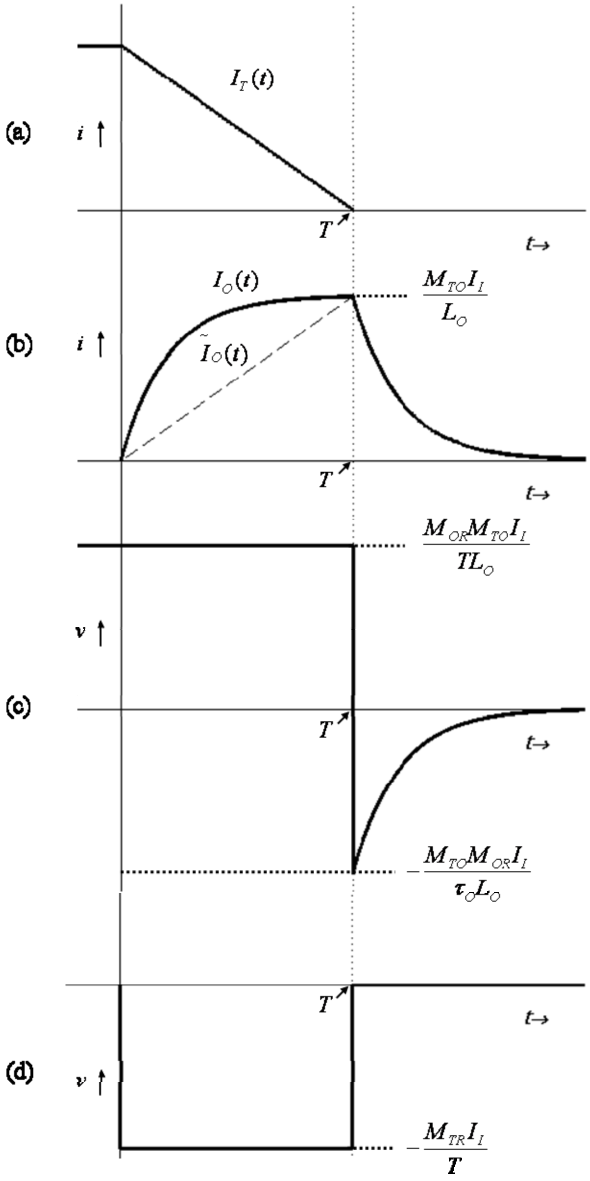

Figure 2.7 Plots for (a) Transmitter Current (b) Object Current (c) Object Coupled Receiver Voltage and (d) Direct Coupled Receiver Voltage. Dotted vertical line marks the time t=T.

The object current, $I_O(t)$, when the switch is in position A can be written as,

$$I_O(t) = k_1 + k_2 e^{-t/\tau_O} \tag{2.2}$$

where $\tau_O = L_O/R_O$ is the time constant of the object. At time t =0, the object current is zero and (2.2) yields $I_O(t=0) = k_1 + k_2$ or

$$k_1 = -k_2 \tag{2.3}$$

If the switch was left in position A indefinitely, the current would asymptotically approach V_{OBJECT}/R_O so

$$I_O(t=\infty) = \frac{V_{OBJECT}}{R_O} = k_1 \tag{2.4}$$

Using (2.3) and (2.4) in (2.2) yields,

$$I_O(t) = \frac{M_{TO} I_I}{TR_O}(1 - e^{-t/\tau_O}) \tag{2.5}$$

which is the charge up current of the object, valid only for 0 ≤ t ≤ T. The object current reaches a maximum value at time T, given by,

$$I_O(t=T) = \frac{M_{TO} I_I}{TR_O}(1 - e^{-T/\tau_O}) \tag{2.6}$$

At time t = T, the voltage induced in the object becomes zero, as the transmitter current no longer changes. Therefore, the peak object current given in (2.6) starts to decay exponentially toward zero, starting at time t = T. When the switch in Figure 2.6 is in position ‘B’ ($T \le t \le \infty$), the object current is given by,

$$I_O(t) = \frac{M_{TO} I_I}{TR_O}(1 - e^{-T/\tau_O}) e^{-(t-T)/\tau_O} u(t-T) \tag{2.7}$$

where u(t) is the unit step function. The peak object current in (2.6) can also be expressed as,

$$I_O\left(\frac{T}{\tau_O}\right) = \frac{M_{TO} I_I}{L_O} \frac{(1 - e^{-T/\tau_O})}{\frac{T}{\tau_O}} \tag{2.8}$$

where $\tau_O=L_O/R_O$. If $\frac{M_{TO}I_I}{L_O}$ is taken as a constant, then the peak object current at time t = T takes the form,

$$y(x)=\frac{1-e^{-x}}{x} \tag{2.9}$$

with $x=T/\tau_O$. By L'Hopital's rule, y(x) is maximum when $x=T/\tau_O=0$ or when the current shutoff time is much less than the time constant of the object, $T \ll \tau_o$. Therefore, the turn off time of the transmitter current should be much less than the object time constant to maximize the object current. It is also important that turn off be free of oscillations in addition to being fast. Very fast turn off is not desirable if oscillations exists. Also a linear turn off is superior to exponential turn off because the exponential function only approaches zero after a very long time (approximately five time constants). A low conductivity background and clutter have fast decay rates and therefore by adjusting transmitter current turn-off time T their response can be suppressed in comparison to large objects that have long time constants [4].

2.2.2 Open circuited voltage at the receiver

The voltage at the receiver can be defined in a similar manner as the voltage induced in the object was defined in section 2.2.1. Thus, by Faraday's law the voltage at the receiver is given as

$$V_{OR}=M_{OR}\frac{dI_O(t)}{dt} \tag{2.10}$$

If $T/\tau_o \ll 1$, then a Taylor series expansion of (2.5) provides a linear approximation,

$I_O(t) = \frac{M_{TO} I_I}{TL_O} t$ for the object current during the time $0 \le t \le T$, which is shown in

Figure 2.7(b) as the dashed line. Substituting $\tilde{I}_O(t)$ in (2.10) gives

$$V_{OR}(t) = \frac{M_{OR} M_{TO} I_I}{L_O T}, \ 0 \le t \le T \tag{2.11}$$

Similarly substituting (2.7) in (2.10) for $T \le t \le \infty$ gives

$$V_{OR}(t) = -\frac{M_{TO} M_{OR} I_I}{\tau_O T R_O}(1 - e^{-T/\tau_O}) e^{-(t-T)/\tau_O}, \ T \le t \le \infty \tag{2.12}$$

Using a Taylor series expansion in (2.12), the voltage induced in the receiver coil for $t \ge T$ can be written as

$$V_{OR}(t) = -\frac{M_{TO} M_{OR} I_I}{\tau_O L_O} e^{-t/\tau_O}, \ t \ge T \tag{2.13}$$

It can be noticed that the ratio of the voltages in (2.11) and (2.13), is τ_o/T and since $\tau_o/T >> 1$, the receiver voltage drops rapidly from the maximum value to the lower limit at $t=T$, and then the exponential decay starts, as indicated in Figure 2.7(c). There is also a direct coupled voltage at the receiver coil due to the coupling between the transmitter and receiver. The direct coupled voltage can be given as

$$V_{DIRECT} = -M_{TR} \frac{d}{dt} I_T(t) = \begin{cases} 0 & t < 0 \\ \frac{M_{TR} I_I}{T} & 0 \le t \le T \\ 0 & t > T \end{cases} \tag{2.14}$$

As mentioned earlier, using a figure eight coil the direct coupling component can be greatly reduced and if the residual coupling between the transmitter coil and the receiver coil is denoted as M_{TR}^{r} (where the superscript r represents residual) then

$$V_{\infty}^{r}(t) = \pm M_{TR}^{r} \frac{dI_T(t)}{dt} \tag{2.15}$$

The sign depends upon the winding direction of the halves of the receiver coil with respect to that of the transmitter coil and upon which half has the larger direct coupling. Therefore direct-coupled voltage can add or subtract from the object coupled receiver voltage for times 0≤t≤T [4-5].

2.3 Summary

In this chapter the basic operating principle of an EMI sensor was introduced and circuit analysis was employed to describe the operational characteristics of a time domain EMI system. Also the importance of clean (without oscillation) turn-off of the transmitter current pulse is stressed which if not obtained can lead to distortion in the object response. In the next chapter a frequency domain analysis of EMI sensors is presented. Also some of the important issues related to methods of measuring the object response will be addressed. Finally specific hardware used to construct a pulsed EMI sensor will be discussed.

CHAPTER 3

HARDWARE IMPLEMENTATION OF EMI SENSOR

In this chapter frequency domain analysis will be used to derive the transfer function that describes both voltage and current measurements of a nonmagnetic finitely conducting object.

3.1 CW EMI System

As mentioned earlier a CW system usually employs a discrete set of sine waves to excite the transmitter coil. In general higher frequencies provide better sensitivity than lower frequencies but lower frequencies penetrate deeper into the metallic objects (due to reduced skin effect) and thus provide more information about the internal structure of an object [8].

3.1.1 Receiver current and output voltage expressions in frequency domain

Referring to Figure 2.4 for CW systems, if the source drives a current I_T through the transmitter coil resistance and inductance R_T and L_T, respectively, and the coupling between the transmitter coil and object, and object and receiver coil can be denoted by M_{TO} and M_{OR}, respectively, then the object current can be written as [10]

$$I_O = \frac{j\omega M_{TO} I_T}{R_O + j\omega L_O} \tag{3.1}$$

Also the transmitter current can be written as

$$I_T = \frac{V_S}{R_T + j\omega L_T} \tag{3.2}$$

where V_S is the source voltage. Substituting (3.2) in (3.1) yields

$$I_O = \frac{j\omega M_{TO}}{(R_O + j\omega L_O)} \frac{V_S}{(R_T + j\omega L_T)} \tag{3.3}$$

The receiver current is given as the voltage induced in the receiver coil divided by the sum of the receiver coil impedance and load impedance or

$$I_R = \frac{j\omega M_{OR} I_O}{(R_R + j\omega L_R + Z_L)} \tag{3.4}$$

Substituting (3.3) in (3.4) we get

$$I_R = \frac{j\omega M_{OR}}{(R_R + j\omega L_R + Z_L)} \frac{j\omega M_{TO}}{(R_O + j\omega L_O)} \frac{V_S}{(R_T + j\omega L_T)} \tag{3.5}$$

Similarly the output voltage across the load is the product of the receiver current and load impedance or

$$V_{out} = \frac{j\omega M_{OR} Z_L}{(R_R + j\omega L_R + Z_L)} \frac{j\omega M_{TO}}{(R_O + j\omega L_O)} \frac{V_S}{(R_T + j\omega L_T)} \tag{3.6}$$

In the case of a receiver current measurement (instead of receiver voltage measurement) the load is assumed short circuited and thus Z_L can be assumed zero. Using this assumption in (3.5) we get

$$I_R = \frac{j\omega M_{OR}}{(R_R + j\omega L_R)} \frac{j\omega M_{TO}}{(R_O + j\omega L_O)} \frac{V_S}{(R_T + j\omega L_T)} \tag{3.7}$$

or

$$I_R = \frac{M_{OR}M_{TO}V_S}{L_O L_R} \frac{j\omega/\omega_O}{(1+j\omega/\omega_O\ )} \frac{j\omega/\omega_R}{(1\ +j\omega/\omega_R\ )}\ \frac{V_S/R_T}{(1+j\omega/\omega_T\ )} \tag{3.8}$$

Where, $\omega_O = R_O/L_O$, $\omega_T = R_T/L_T$ $\omega_R = R_R/L_R$ are object, transmitter and receiver coil break frequencies, respectively. In a voltage measurement, if Z_L is very high (open circuit receiver coil) (3.6) may be written as

$$V_{out} = \frac{j\omega M_{TO}M_{OR}}{(R_O + j\omega L_O)} \frac{j\omega V_S}{(R_T + j\omega L_T)} \tag{3.9}$$

or

$$V_{out} = \frac{M_{OR}M_{TO}V_S}{L_T L_R} \frac{j\omega/\omega_T}{(1+j\omega/\omega_T)} \frac{j\omega/\omega_O}{(1+j\omega/\omega_O)} \tag{3.10}$$

Actually, in practice if the load is made too large, current will be forced to flow in the parasitic receiver coil capacitance and undesirable ringing or oscillations will occur. To avoid oscillations the receiver coil is usually terminated in a resistance Rshunt that leads to the following modified form of (3.6) :

$$V_{out} = \frac{M_{OR}M_{TO}V_S}{L_T L_R} \frac{j\omega/\omega_T}{(1+j\omega/\omega_T)} \frac{j\omega/\omega_O}{(1+j\omega/\omega_O)} \frac{R_{shunt}}{((R_R + R_{shunt}) + j\omega L_R} \tag{3.11}$$

One can see from (3.8) that in a receiver current measurement the receiver coil behaves as a high pass filter while the transmitter filter characteristics are low pass. Important discrimination information is present in the late time response. Therefore, it is desirable to shift the 3 dB point of the receiver coil to as low a frequency as possible. The break frequency (f_R) of the receiver coil is inversely proportional to the number of turns on the receiver coil. Therefore, increasing the number of turns will decrease the break frequency. However, a point is reached where increasing the number of turns does not significantly lower the break frequency (a point of diminishing return is reached). As discussed in the next section compensation circuitry may be employed to further reduce the break frequency. In a voltage measurement, however the transmitter coil displays high pass filter characteristics while the receiver displays low pass filter characteristics due to which a compensation circuit on the receiver side is not required. Also, the number of turns for a low pass receiver coil in a voltage measurement is usually much less than that for a high pass receiver coil for a current measurement.

3.1.2 Receiver current measurement using current-to-voltage converter and compensation circuit

Figure 3.1 shows the circuit diagram of a current-to-voltage converter that is used for current measurements. The two halves of the receiver coil are wound in opposite directions so that direct coupling between transmitter and receiver coils is minimized (ideally zero). The receiver coil that is used has a break frequency of 10 Hz and as explained above acted as a high pass filter for current measurements. A simple RC filter circuit that has a cut off frequency of 10 Hz may be used to model the receiver coil frequency response. A numerical circuit analysis software called Pspice[3.1] was used to compute the response. The input current from the coil is assumed to be 10 mA which gives an output voltage of 2V. In accordance with operational amplifier theory the gain of current-to-voltage converter is given as $(R_3 + R_2)$ or 200. The output voltage of the current-to-voltage converter is given by $V_{out} = I_{in}(R_3 + R_2)$. Figure 3.2 and 3.3 provide plots of the input current and output voltage as obtained from the Pspice.

[3.1] Pspice was developed by MicroSim which was acquired by Orcad and now belongs to Cadence Design Systems. For more information please visit www. Cadence.com

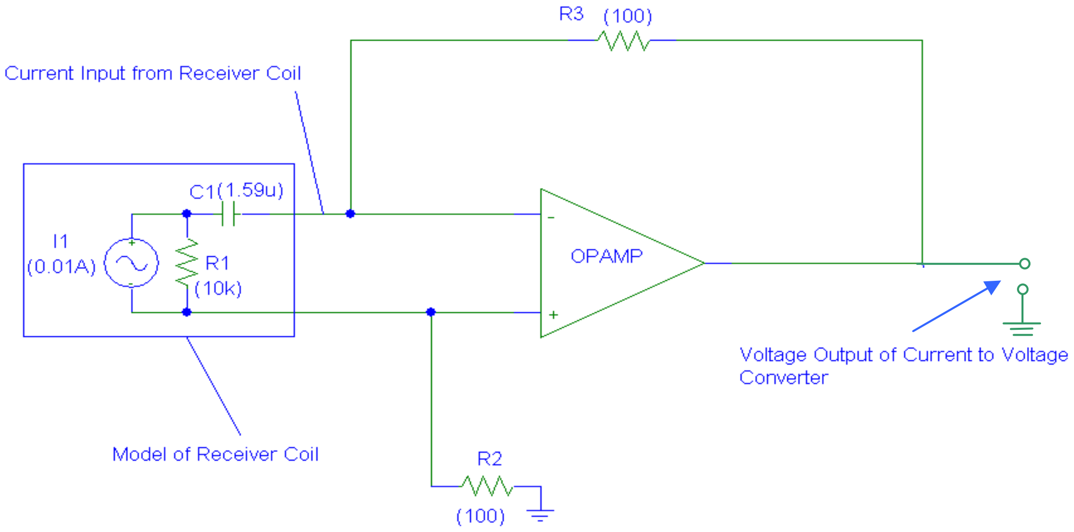

Figure 3.1 Current-to-voltage converter with gain of 200.

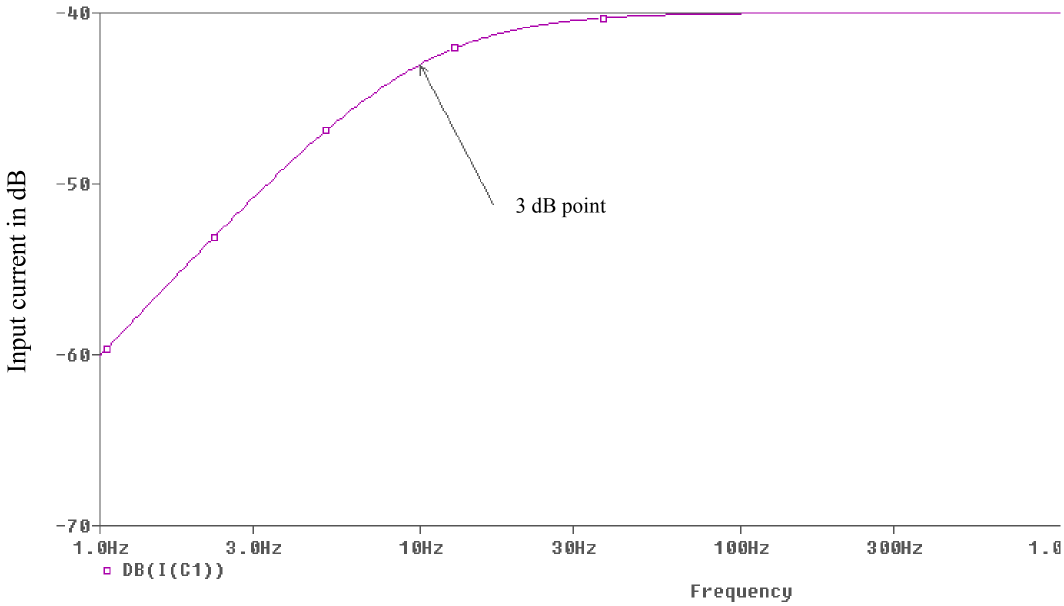

Figure 3.2 Input current in dB from the receiver coil.

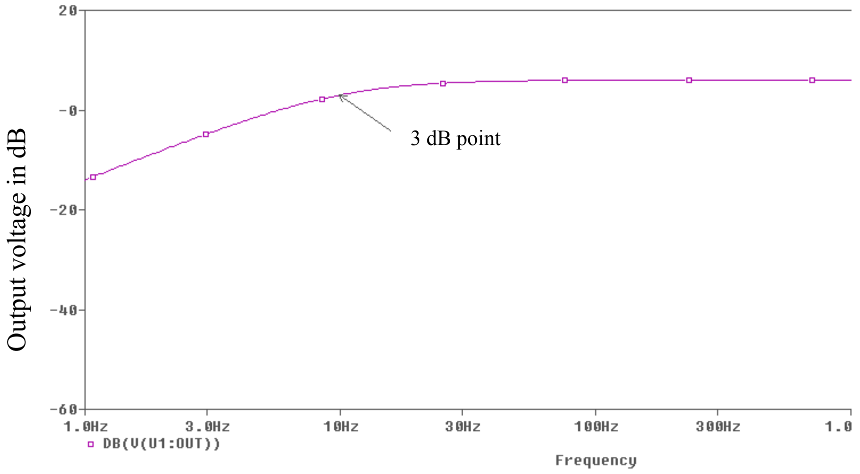

Figure 3.3 Output voltage in dB from differential current-to-voltage converter with 3 dB point at 10 Hz.

A compensation circuit may be used to shift the 3 dB break frequency lower in order to achieve the desired late time response [4], [11]. The final circuit configuration is shown in Figure 3.4. In this circuit the actual break frequency of the coil is given as $f_{break}(actual) = \frac{1}{2\pi R_1 C}$ and the desired break frequency is given as $f_{break}(desired) = \frac{1}{2\pi R_2 C}$. Thus R_2 has to be as large as possible. The gain at higher frequencies is determined by R_1 and is equal to $2R_1$. The actual break frequency of the coil is 10 Hz and at arbitrarily high frequencies a gain of 200 is required. Therefore R_1 is set to 100 ohms and thus C can be determined using $f_{break}(actual) = \frac{1}{2\pi R_1 C}$. Similarly the desired break frequency is chosen as 0.1Hz and therefore R_2 can be calculated using $f_{break}(desired) = \frac{1}{2\pi R_2 C}$ which gives R_2 =10K ohms. Figure 3.5 shows frequency response of the output voltage from the compensated circuit. The input current frequency response is the same as shown in Figure 3.2.

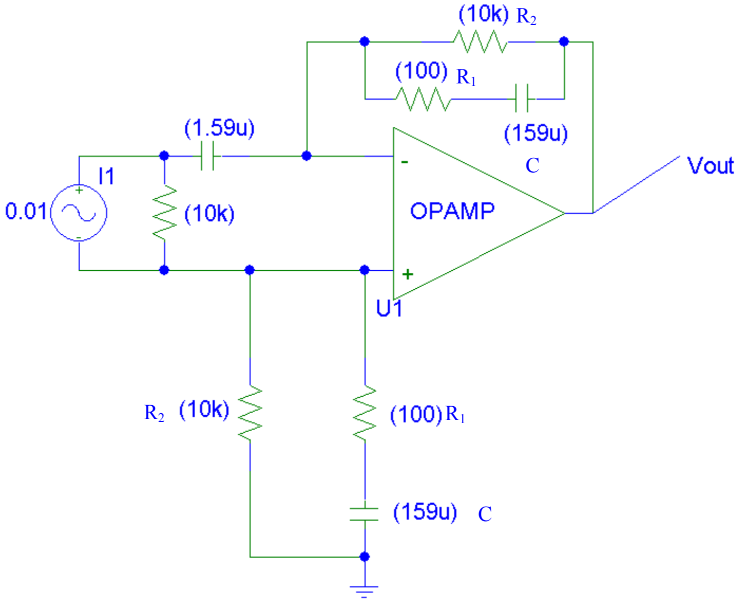

Figure 3.4 Current-to-voltage converter with compensation circuit.

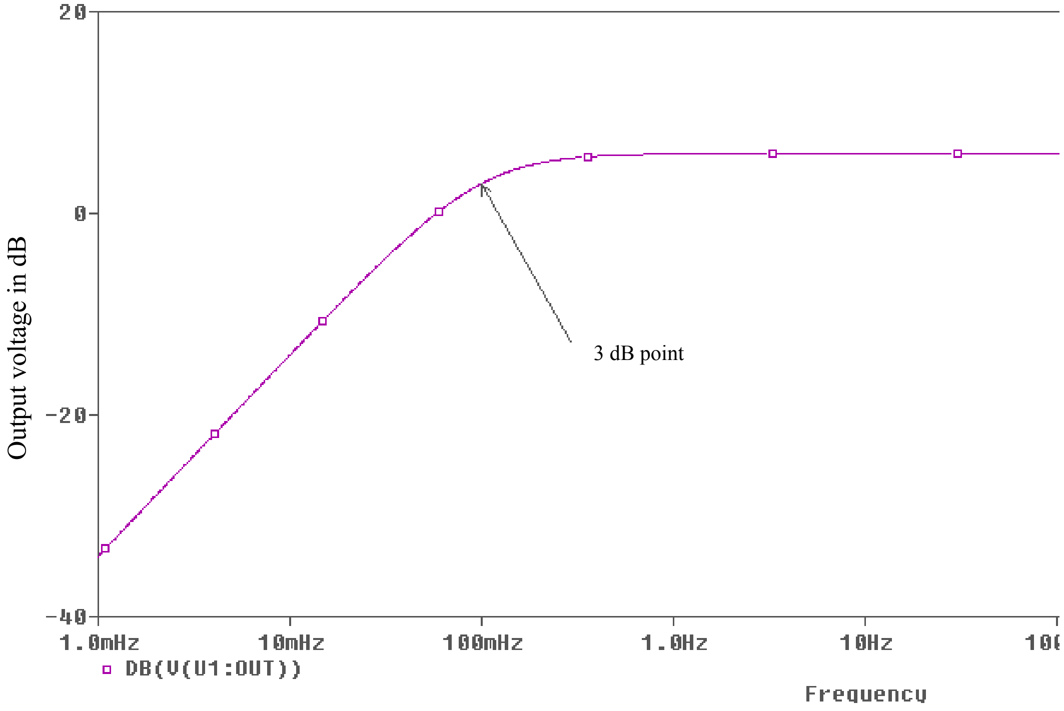

Figure 3.5 Frequency response of output voltage in dB from current-to-voltage converter with compensation circuit. The 3dB point is shifted from 10 Hz to 100 mHz.

3.1.3 Analytical explanation of compensation circuit

The total impedance Z across the compensation circuit shown in Figure 3.6 is given as

$$Z = \frac{\left(R_1 + \frac{1}{j\omega C_1}\right)R_2}{R_1 + R_2 + \frac{1}{j\omega C_1}} \tag{3.12}$$

After rearranging terms, (3.12) can also be written as

$$Z = \frac{R_1 R_2}{R_1 + R_2}\left(\frac{1 + \frac{1}{j\omega C_1 R_1}}{1 + \frac{1}{j\omega C_1\left(R_1 + R_2\right)}}\right) \tag{3.13}$$

Assuming $R_2 » R_1$, (3.13) reduces to

$$Z = R_1\left(\frac{1 + \frac{1}{j\omega C_1 R_1}}{1 + \frac{1}{j\omega C_1 R_2}}\right) \tag{3.14}$$

or

$$Z = R_1\left(\frac{j\omega + \frac{1}{C_1 R_1}}{j\omega + \frac{1}{C_1 R_2}}\right) \tag{3.15}$$

Expressing (3.15) in terms of the laplace frequency domain variable s yields

$$Z = R_1\left(\frac{s + \frac{1}{C_1 R_1}}{s + \frac{1}{C_1 R_2}}\right) \tag{3.16}$$

Thus from (3.16) one may observe that the pole of the response is set by $R_2 C_1$ and the zero by $R_1 C_1$. Thus

$$f_Z = \frac{1}{2\pi R_1 C_1} \tag{3.17}$$

and

$$f_P = \frac{1}{2\pi R_2 C_1} \tag{3.18}$$

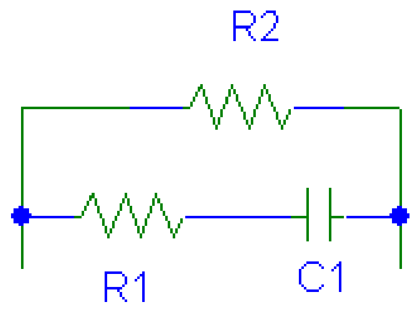

Figure 3.6 A compensation circuit that compensates for the roll off at 20dB/decade of the low frequency response of the receiver coil.

Figure 3.7 shows the plot of the gain in dB versus frequency with f_p=0.1Hz and f_Z=10 Hz. From the figure we can see that there is a 20 dB/decade roll off between the pole and zero frequencies.

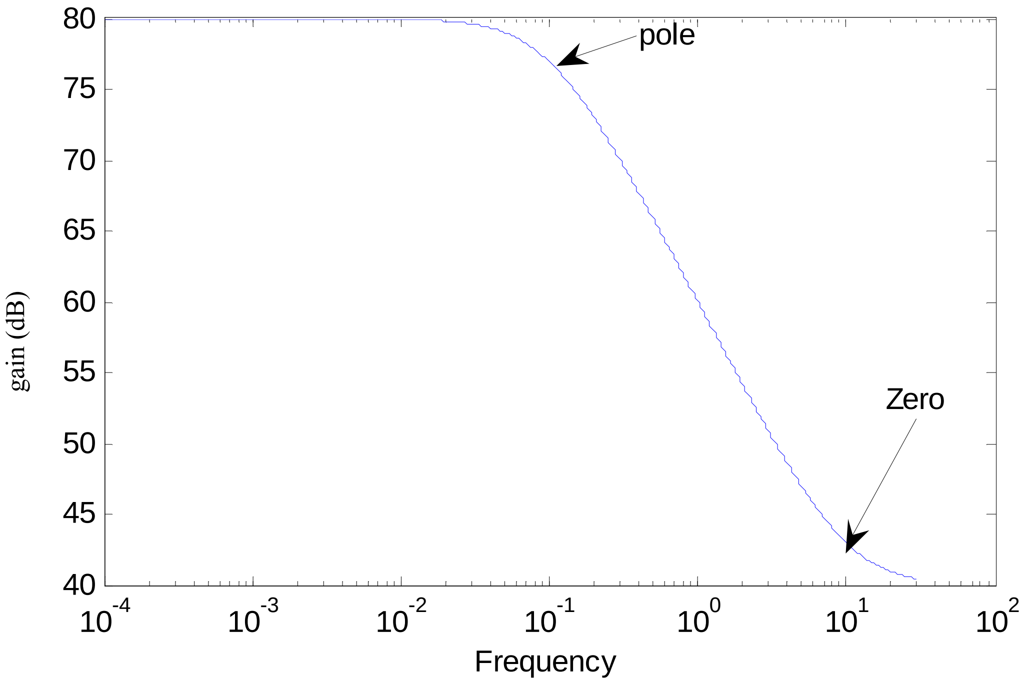

Figure 3.7 Plot of gain in dB versus frequency for the compensation circuit.

Since the receiver coil current has high a pass filter characteristic with a cut off frequency of 10 Hz below which its response increases by 20 db/decade, the roll off of the compensation circuit will exactly cancel this increase thereby pushing the receiver coil current break frequency to 0.1 Hz. Figure 3.8 shows a plot of the phase of the compensated circuit in degrees versus frequency. From this plot one can observe that at the pole and zero frequencies the phase is 45 degrees. From (3.16) it can also be seen that the low frequency gain of the compensation circuitry depends on R_2 and to shift the pole frequency lower by a decade, R_2 has to be made 10 times greater. Increasing the gain at lower frequencies limits the bandwidth of the opamp by an amount that is dependent upon the opamp's gain bandwidth product.

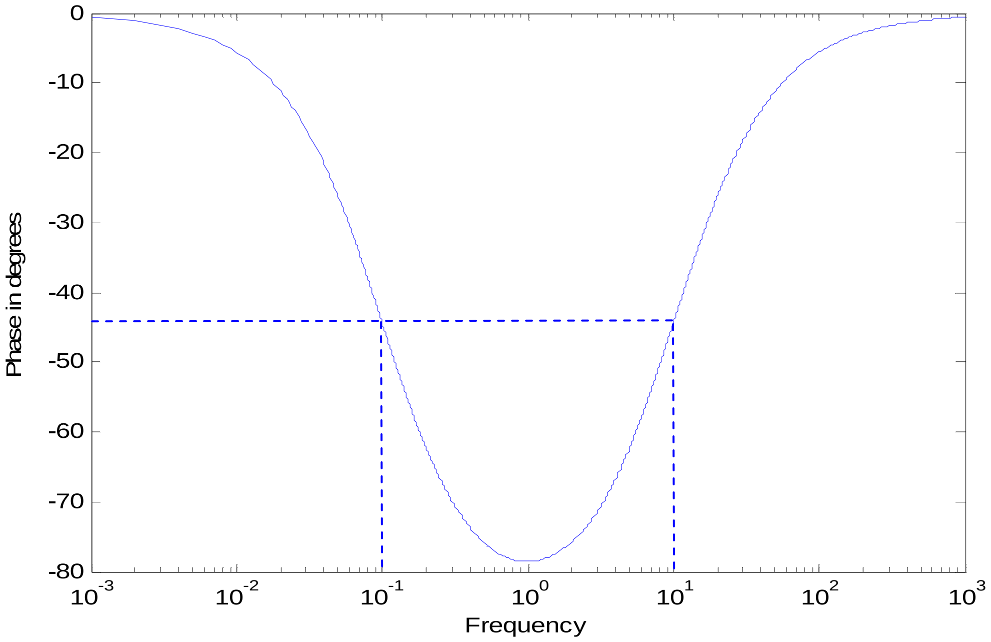

Figure 3.8 Plot of compensated circuit phase in degrees versus frequency.

3.1.4 Receiver voltage measurement using voltage amplifier

According to Figure 3.9, the voltage amplifier is built using a non inverting opamp configuration so that the receiver coil is terminated in a large resistance. Without Rshunt some frequency will be reached where all the coil current will flow in the parasitic capacitance because of the large resistance between the positive terminal of the opamp and ground. From (3.11) it can be seen that the receiver coil frequency response is low pass while the object response is high pass. Therefore, it is desirable to shift the receiver coil break frequency as high as possible so that object response is not attenuated above the 3 dB point of the receiver coil. The break frequency of the receiver coil is modified due to R_{shunt} to $f_{break} = \frac{R_R + R_{shunt}}{L_R}$. Thus by making R_{shunt} very large, a higher break frequency can be achieved but R_{shunt} can’t be too large or current will flow in the parasitic capacitance of the coil resulting in oscillations. When R_{shunt} is made large in comparison to the impedance of the parasitic coil capacitance a certain frequency will be reached above which currents will start flowing in the parasitic coil capacitance that forms a resonant circuit composed of L_R, R_R and C(parasitic). Under this condition Vin will increase proportionally with frequency at 20 dB/dec up-to the first self-resonance frequency of the receiver coil (typically around 10 kHz). This in-turn distorts the output voltage, which is no longer a faithful representation of the object response. Figure 3.10 shows Vin versus frequency for different values of R_{shunt} with respect to C(parasitic).

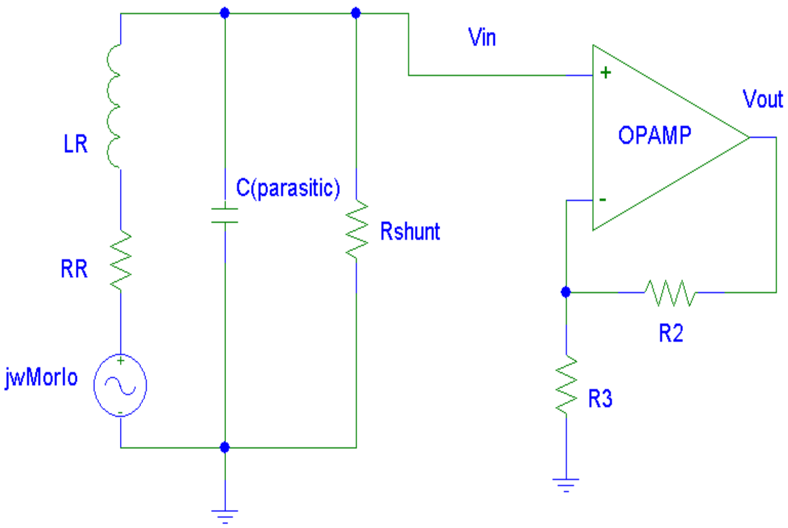

Figure 3.9 Voltage amplifier in non inverting configuration connected to receiver coil. The gain of the amplifier is given by $\left(1+\frac{R_2}{R_3}\right)$.

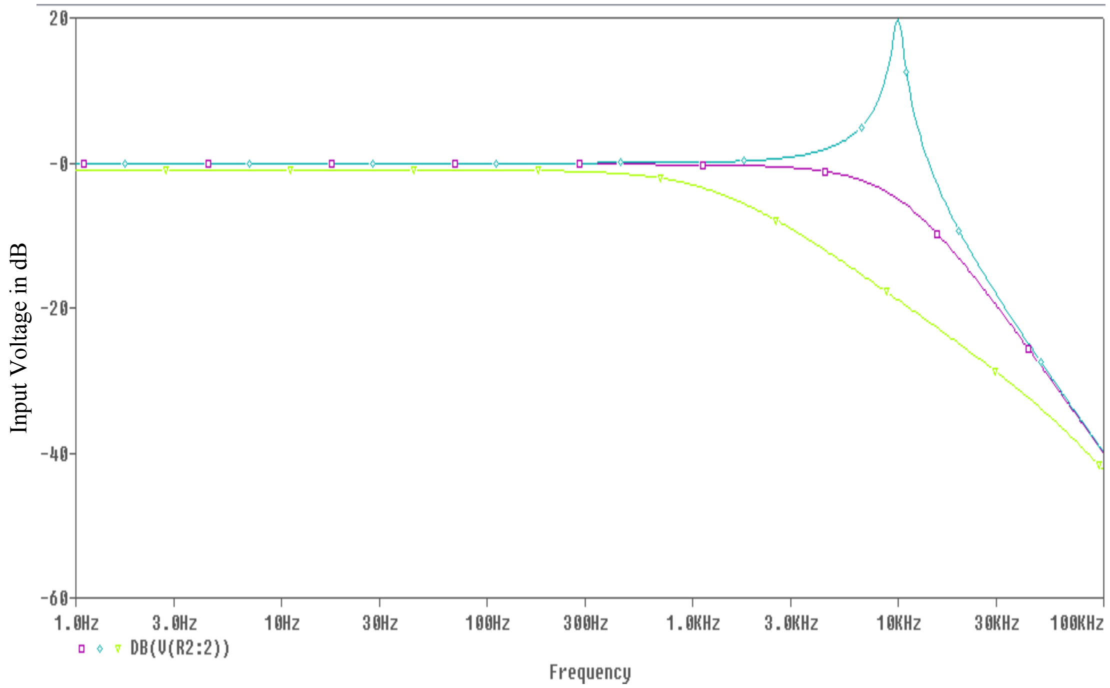

Figure 3.10 Plot of Vin versus frequency. Pink curve shows critically damped response. Light green curve is for R_{shunt} < C(parasitic) and dark green curve is for R_{shunt} >> C(parasitic). Resonance frequency of the coil is set to 10 KHz.

3.2 Receiver current expression in time domain

According to Figure 3.11 the circuit equations for both object and receiver current after the transmitter current turn off can be written as

$$j\omega L_O I_O + R_O I_O + j\omega M_{OR} I_R = K \tag{3.19}$$

and

$$j\omega L_R I_R + R_R I_R + j\omega M_{OR} I_O = 0 \tag{3.20}$$

where K $= L_O I_O^-$ and I_O^- is the steady state object current just before transmitter current turn off and I_O and I_R are object and receiver coil currents after transmitter current turn off. Writing (3.19) and (3.20) in matrix form results in

$$\begin{bmatrix} (j\omega L_O + R_O) & j\omega M_{OR} \\ j\omega M_{OR} & (R_R + j\omega L_R) \end{bmatrix} \begin{bmatrix} I_O \\ I_R \end{bmatrix} = \begin{bmatrix} K \\ 0 \end{bmatrix} \tag{3.21}$$

Thus I_R can be written as

$$I_R = \frac{\begin{bmatrix} (j\omega L_O + R_O) & K \\ j\omega M_{OR} & 0 \end{bmatrix}}{\begin{bmatrix} (j\omega L_O + R_O) & j\omega M_{OR} \\ j\omega M_{OR} & (R_R + j\omega L_R) \end{bmatrix}} \tag{3.22}$$

Expanding (3.22) in terms of the laplace transfer variable s yields

$$I_R = \frac{-KsM_{OR}}{\left[(sL_O + R_O)(R_R + sL_R)\right] - (sM_{OR})^2} \tag{3.23}$$

Since M_{OR} is very small therefore neglecting its square in (3.23) leads to

$$I_R = \frac{-KsM_{OR}}{\left[(sL_O + R_O)(R_R + sL_R)\right]} \tag{3.24}$$

or

$$I_R = \frac{-KsM_{OR}}{L_O L_R\left[(s+\frac{R_O}{L_O})(s+\frac{R_R}{L_R})\right]} \tag{3.25}$$

Expanding in terms of partial fractions leads to

$$I_R = \frac{\frac{KM_{OR} f_R}{L_O L_R(-f_R+f_O)}}{(s+f_R)} + \frac{\frac{KM_{OR} f_O}{L_O L_R(f_R-f_O)}}{(s+f_O)} \tag{3.26}$$

where $f_R = \frac{R_R}{L_R}$ and $f_O = \frac{R_O}{L_O}$

or

$$I_R = \frac{KM_{OR}}{L_O L_R(-f_R+f_O)}\left[\frac{f_R}{(s+f_R)} - \frac{f_O}{(s+f_O)}\right] \tag{3.27}$$

Converting (3.27) to time domain results in

$$I_R = \frac{KM_{OR}}{L_O L_R(-f_R+f_O)}\left[f_R e^{-f_R t} - f_O e^{-f_O t}\right] \tag{3.28}$$

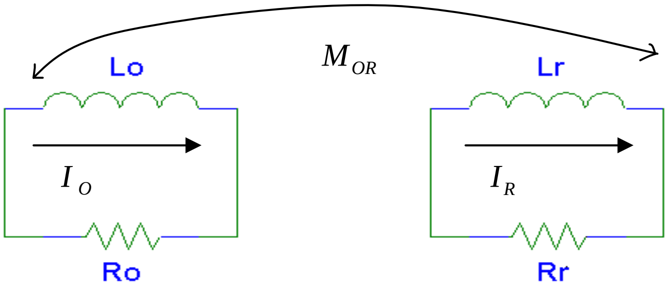

Figure 3.11 Interaction between the receiver and object circuits.

From (3.28) it can be inferred that the receiver current consist of two exponentials with decay rates that depend on the receiver ($\tau_R = \frac{L_R}{R_R}$) and object time constants ($\tau_O = \frac{L_O}{R_O}$).

It was mentioned earlier in connection with the frequency domain analysis that in a current measurement the receiver coil has high pass filter characteristic and therefore a compensation circuit was used to lower its break frequency (specifically from 10 Hz to 0.1 Hz). Thus assuming f_R to be very low as compared to f_O (3.28) can be written as

$$I_R = \frac{KM_{OR}}{L_O L_R}\left[\frac{f_R}{f_O}e^{-f_R t} - e^{-f_O t}\right] \tag{3.29}$$

The information regarding the object is in the exponential that decays with object time constant f_o^{-1}, however the exponential that decays with receiver time constant is small in amplitude and also decays very slowly due to small f_R. Thus in a current measurement the break frequency of the receiver has to be very low to suppress the unwanted receiver time constant exponential so that it does not interfere with the response of the object during the time of collection of data.

From (3.28) the voltage input (Vin) to the voltage amplifier of Figure 3.9 can be written as

$$V_{in} = \frac{KM_{OR}R_{shunt}}{L_O L_R(-f_{break} + f_O)}\left[f_{break}e^{-f_{break}t} - f_O e^{-f_O t}\right] \tag{3.30}$$

if parasitic capacitance effects are neglected. In (3.30) $f_{break} = \frac{R_R + R_{shunt}}{L_R}$ and $f_O = \frac{R_O}{L_O}$.

Since in a voltage measurement the receiver coil behaves as a low pass filter the 3 dB point of the coil has to be high enough so that high pass object response is not distorted. Assuming $f_{break} >> f_O$ (3.30) can be written as

$$V_{in} = \frac{KM_{OR}}{L_O L_R}R_{shunt}\left[-e^{-f_{break}t} + \frac{f_O}{f_{break}}e^{-f_O t}\right] \tag{3.31}$$

Thus from (3.31) it can be noticed that in a voltage measurement f_{break} has to be as high as possible so that unwanted receiver exponential with higher amplitude then object exponential decays quickly and does not interfere with object response. One way to achieve this is to make sure that R_{shunt} is large which is only possible if C (parasitic) is small so that resonance is avoided. C (parasitic) can be reduced by decreasing the number of turns of the receiver coil or by modifying the receiver coil geometry.

As in voltage measurement, receiver response decays quickly and does not interfere with the object late time response which is critical for discrimination purposes. It can be concluded that in general a voltage measurement is much better than a current measurement. However, if the dynamic range of response of an object is large then the more effective method depends upon the break frequency of the receiver coil with respect to object break frequency and also upon the time window over which the data is collected. For illustration purpose, if we consider f_R= 0.1 and f_O=1000 and the time window for data collection is 20 ms then the plot of normalized I_R for a current measurement is shown in Figure 3.12(a).

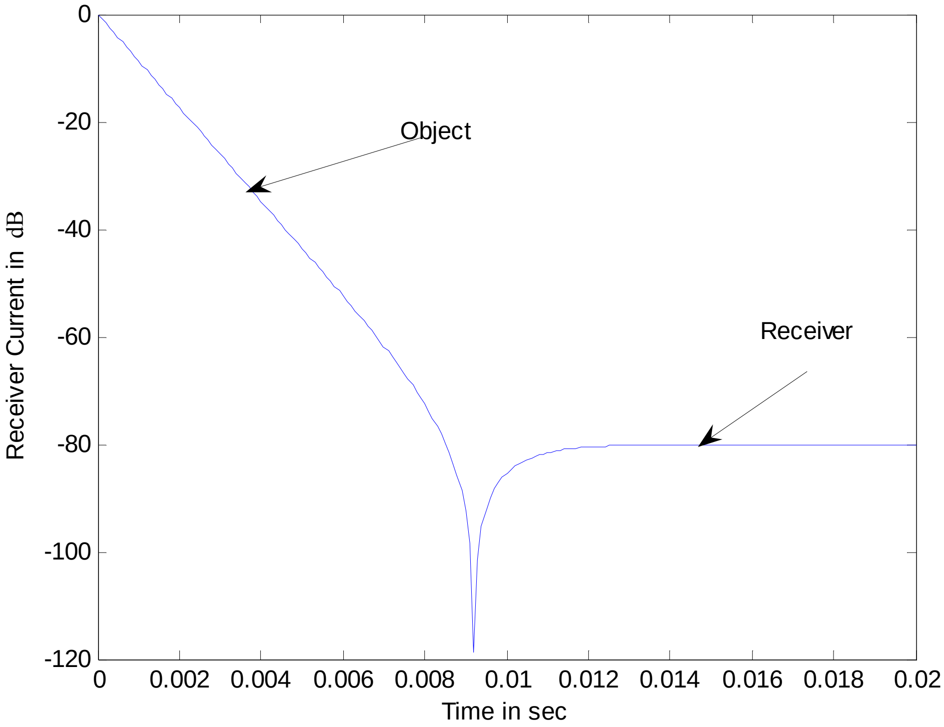

Figure 3.12a Plot of normalized receiver current versus time for current measurement with f_R= 0.1Hz and f_O =1000 Hz.

For a voltage measurement considering f_R= 10000 and f_O =1000 Hz, the receiver response is as shown in Figure 3.12(b). Clearly form Figure 3.12(a) and (b) it can be inferred that a voltage measurement provides a larger object dynamic range.

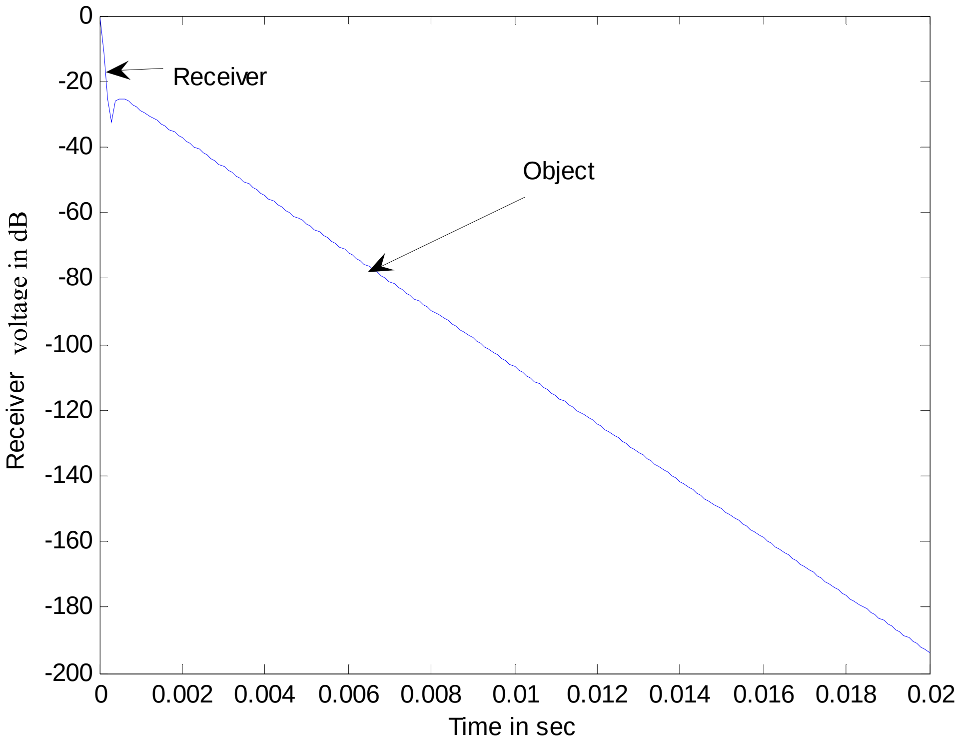

Figure 3.12b.Plot of normalized receiver voltage versus time with f_R= 10000 Hz and f_O =1000 Hz.

3.3 Summary

In this chapter voltage and current measurement methods are compared using continuous wave EMI system analysis. Also a detailed explanation of the compensation circuit needed in a current measurement is discussed. In either case (voltage or current measurement) a low pass filter can be used to eliminate high frequency noise. In the next chapter the hardware configuration of the EM63 sensor (a commercial sensor) is introduced briefly in order to facilitate comparison of data collected from our sensor and that of the EM 63.

CHAPTER 4

TIME DOMAIN EM63 SENSOR

4.1 General description

The EM63 is a high power, high sensitivity, and wide bandwidth full time domain UXO detector and consists of a powerful transmitter coil that generates a pulsed primary magnetic field which induces eddy currents in nearby metallic objects. The decay of these eddy currents generates a secondary magnetic field with a specific decay rate that is determined by target size, shape, orientation and composition. This secondary magnetic field decay thus contains important information towards complete characterization of the target. Figure 4.1 shows an assembled EM63 sensor [12]. The EM63 measures the complete transient response over a wide dynamic range. Time measurements are recorded at 26 geometrically spaced gates, covering a time range from 180us to 25ms.The data acquisition is supported by the PRO4000 field computer which is able to simultaneously receive GPS data for position control [13].

Figure 4.1 EM63 sensor.

4.2 Major components of the system

The main components of the system are a control console, trailer mounted transmitter coil and sensors, battery pack, preamplifier, acquisition and editing software. The trailer coil assembly consists of a transmitter coil and three receiver coils as shown in Figure 4.1. A bipolar current waveform is used for excitation of the transmitter coil which is $1\text{m}\times 1\text{m}$ in size. The main receiver coil is coincident with the EM63 source and is $0.5\text{m}\times 0.5\text{m}$ in size. The second receiver coil axially mounted with the main coil is used for target depth determination and is 60cm above the main coil and is also $0.5\text{m}\times 0.5\text{m}$ in size. The EM63 control console contains the system computer and associated electronics for drive of the transmitter coil and process signals from the receiver coil preamplifier.

4.3 Data Collection

The gates of EM63 are narrow during the early time of the response when the signal is very strong and become wider during late time because the signal becomes very weak and to get good S/N ratio time gates have to be wider at later times. The data for a target at a particular location is collected in a horizontal row which contains data reading from each of the 26 gates in millivolts. The measuring range of the EM63 extends up to 10,000 mV.

4.4 Summary

The configuration of the EM63 sensor has been discussed briefly with the intent to compare and contrast the response of the EM63 sensor with the response of the sensor developed for this thesis.

CHAPTER 5

TIME DOMAIN EMI SENSOR MEASUREMENTS

In this chapter the configuration of our sensor is described (see Figure 5.1). Measurements of copper rings and spherical targets are acquired with our sensor and the EM63 and the two data sets are compared.

5.1 Measurement Setup

A HP 3314A function generator is used to generate a square wave signal (frequency=50 Hz) which is fed to a Powertron Model 250A (250 watts) power amplifier in order to boost the current flowing through the transmitter coil. A resistor is connected in parallel with the transmitter coil in order to reduce ringing. A Tektronix current probe is used to measure the current flowing in the transmitter and a Tektronix TDS3054B oscilloscope is used for display purposes. Figure 5.1 shows the general block diagram of all the instruments and the connections used to excite the transmitter. For voltage measurements two receiver coils were wrapped in the same direction and connected to provide a single coil with a centre tap (three wire option). The ends of the receiver coil provide inputs to the + and – terminals of a differential amplifier (voltage amplifier) and the center tap was connected to ground as shown in Figure 5.2. The Rshunt must be adjusted to reduce ringing as was described in the previous chapter. Most of the voltage measurements described here were made using a high performance op-amp manufactured by Linear Technology (the LT1028) [14]. For current measurements the receiver coils were wrapped in opposite directions so that the voltage induced from each half cancels each other. The general schematic of the current-to-voltage converter (excluding the compensation circuit) is shown in Figure 5.3.

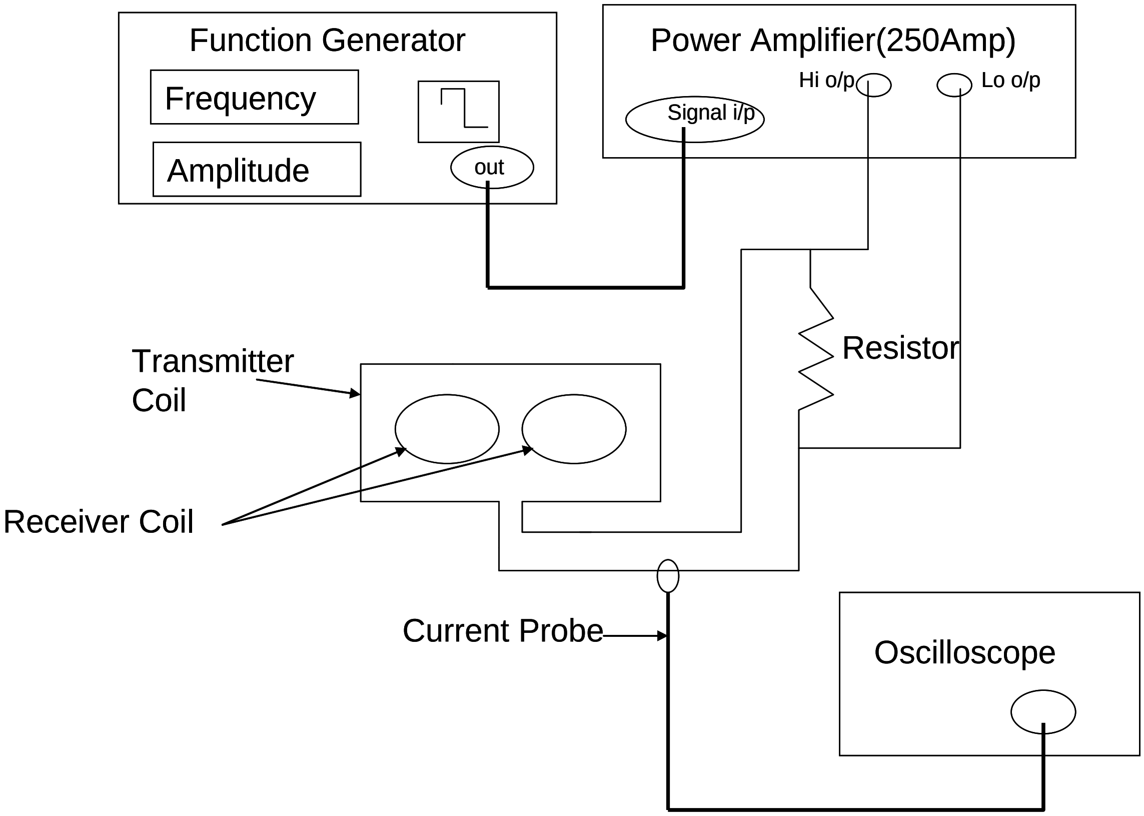

Figure 5.1 Setup used to excite the transmitter coil.

A MAX430 operational amplifier manufactured by MAXIM was used in the current measurements because it has very low input offset and drift as compared to conventional opamps [15]. The output voltage from the two measurements can be analyzed using an oscilloscope or using a data acquisition card installed in a desktop computer. A 16 bit analog to digital PCI bus card (Compuscope (CS) 1602 from Gage

Applied Inc [16]) was installed on a desktop computer and the *Gagescope* data acquisition software was used for storing and displaying data acquired by CS1602. The software also provides controls for changing the sampling rate, trigger level, data points, etc.

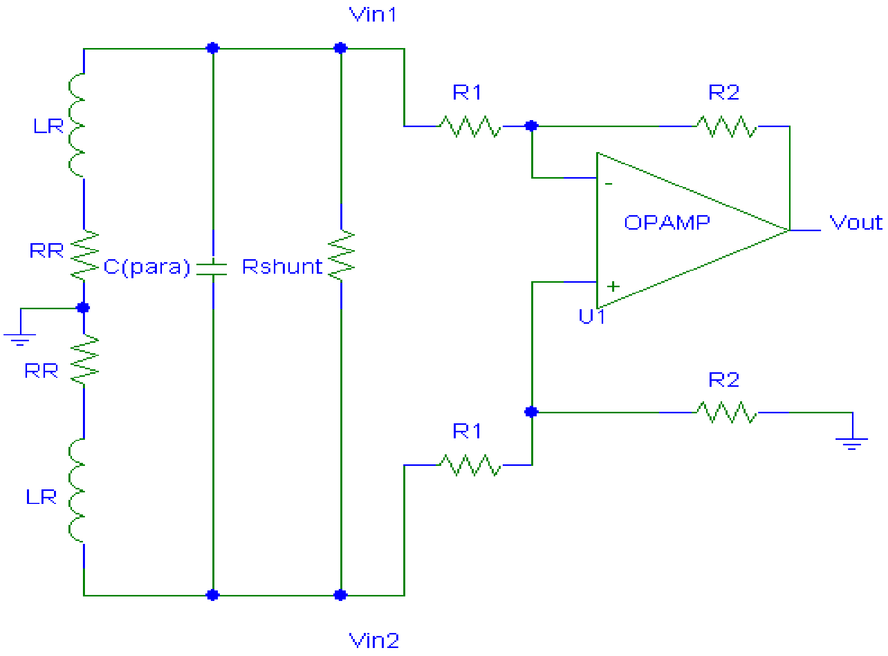

Figure 5.2 Differential voltage amplifier with Vout= $\frac{R_2}{R_1}$ (Vin2-Vin1).

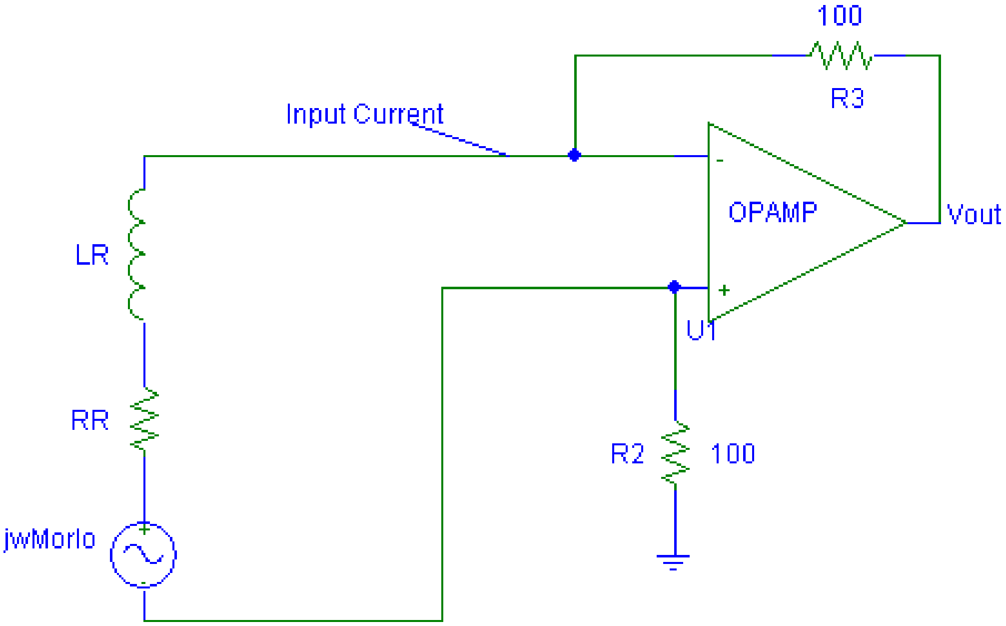

Figure 5.3 Current to voltage converter with Vout=$I_{in}(R2+R3)$.

5.2 Measurements from TD sensors

The first three targets that were used to compare the performance of our sensor to that of the EM63 sensor are three copper rings of approximately the same mean radius but of varying thickness. Their responses are compared with those acquired by the EM63. The small copper ring has the fastest decay rate and therefore has the maximum dynamic range while the large ring has the longest time constant and therefore the least dynamic range. The responses from both current and voltage measurements using our sensor are shown in Figure 5.4 and 5.5.

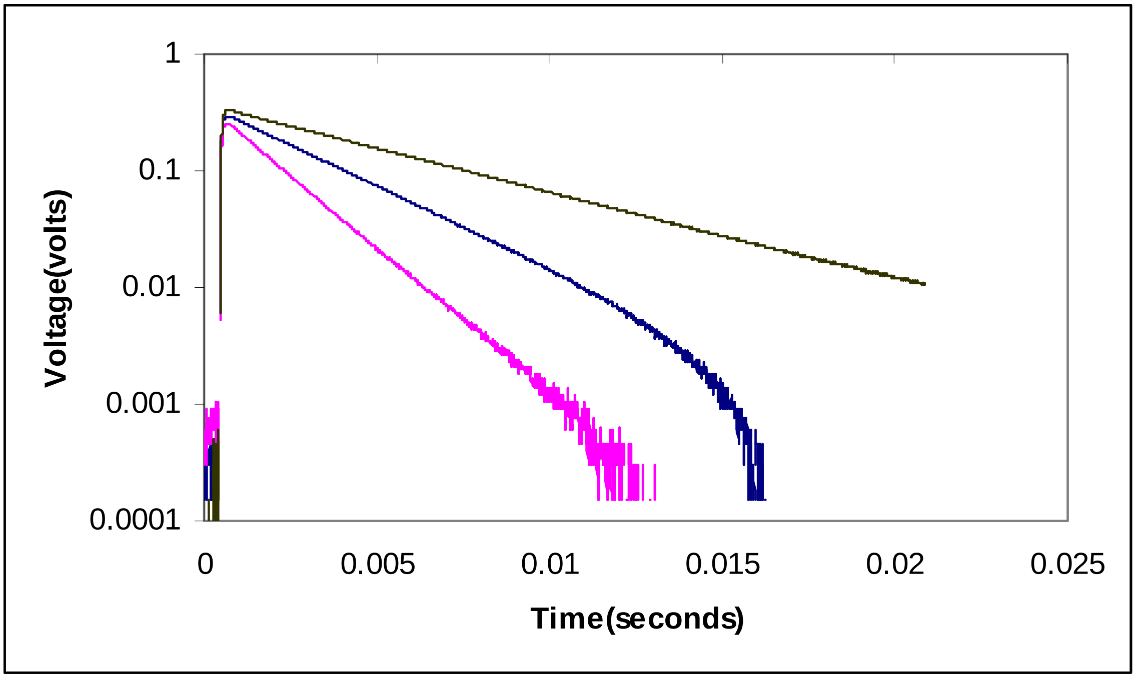

Figure 5.4 Small (Pink curve), medium (Blue Curve) and large (Green Curve) copper ring response with current measurements (Log/Linear).

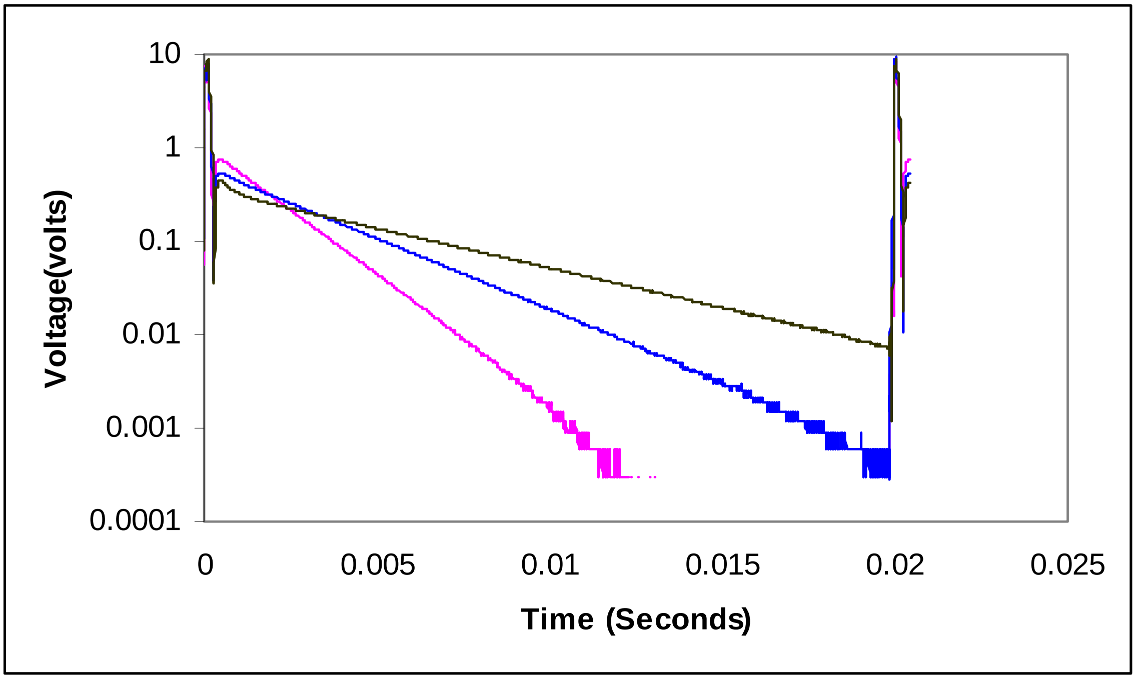

Figure 5.5 Small (Pink curve), medium (Blue Curve) and large (Green Curve) copper ring response with voltage measurements using differential configuration (Log/Linear).

It can be easily seen that the voltage measurement has significantly more dynamic range than the current measurement. This observation is in agreement with the theory presented in the previous chapters. Furthermore, the voltage measurements were taken out of doors while the current measurements were taken in the laboratory and the latter environment probably has more ambient noise (particularly 60 Hz noise). However our sensor response is still inferior to that of the EM63 possibly due to fact that our transmitter turn off response is exponential and slower than the linear current turn off response of the EM63. Figure 5.6 shows a comparison of the EM63 response for small, medium and large copper rings with respect to the response of our sensor.

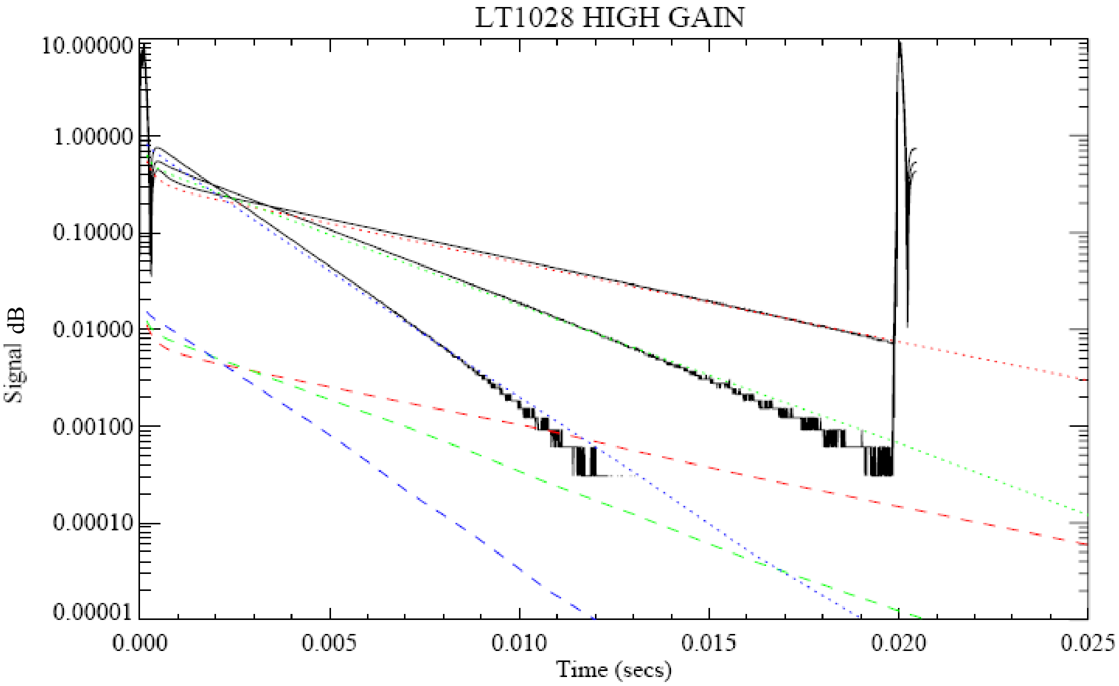

Figure 5.6 Blue, green and red dotted curves are responses from small, medium and large copper rings respectively using EM63 sensor and the corresponding overlapping black curves are from our sensor at 5 inch height. Dashed blue, green and red curves are for 25 inch height using EM63 sensor (Log/Linear).

5.2.1 Response of 4 inch steel sphere

Figure 5.7a compares the response of a 4 inch steel sphere from each sensor. It can be seen from the figure that the sphere response does not have nearly the dynamic range that the copper rings have and therefore the two measurements are in good agreement. Figure 5.7b presents the same information in log versus log scale.

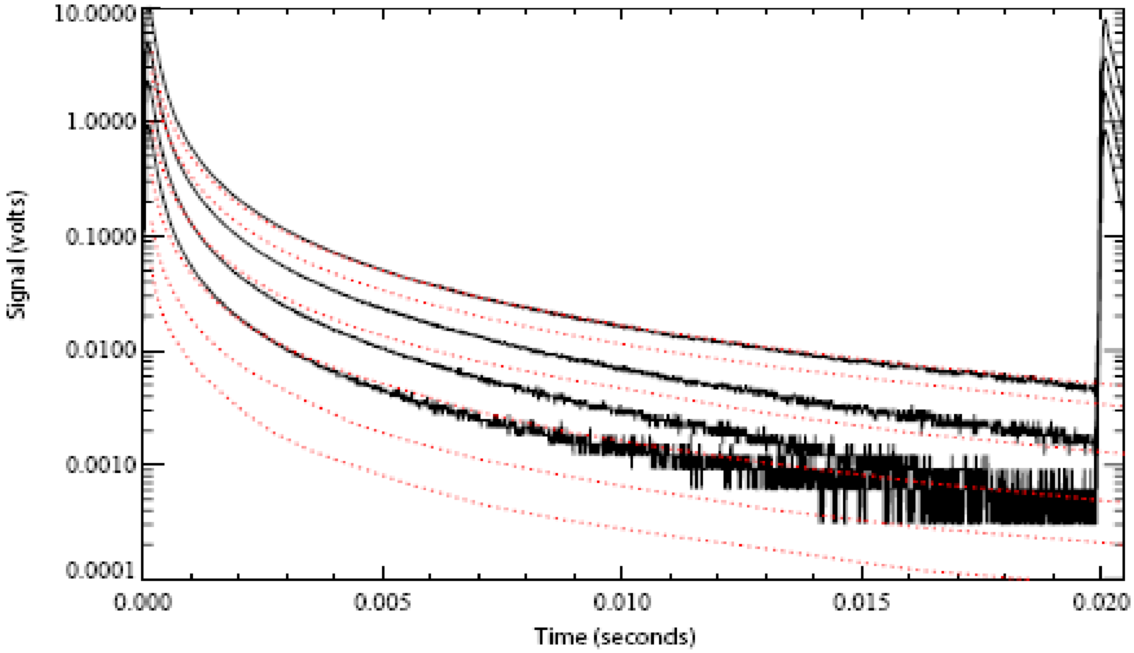

Figure 5.7a Black curves are responses of 4 inch steel sphere from our sensor using high gain INA103KP instrumentation amplifier in voltage measurement method at heights of 3, 6, 9 and 12 inches respectively and red dotted curves are from EM63 at heights of 2.5, 5, 10, 15 and 20 inches respectively (Log/Linear).

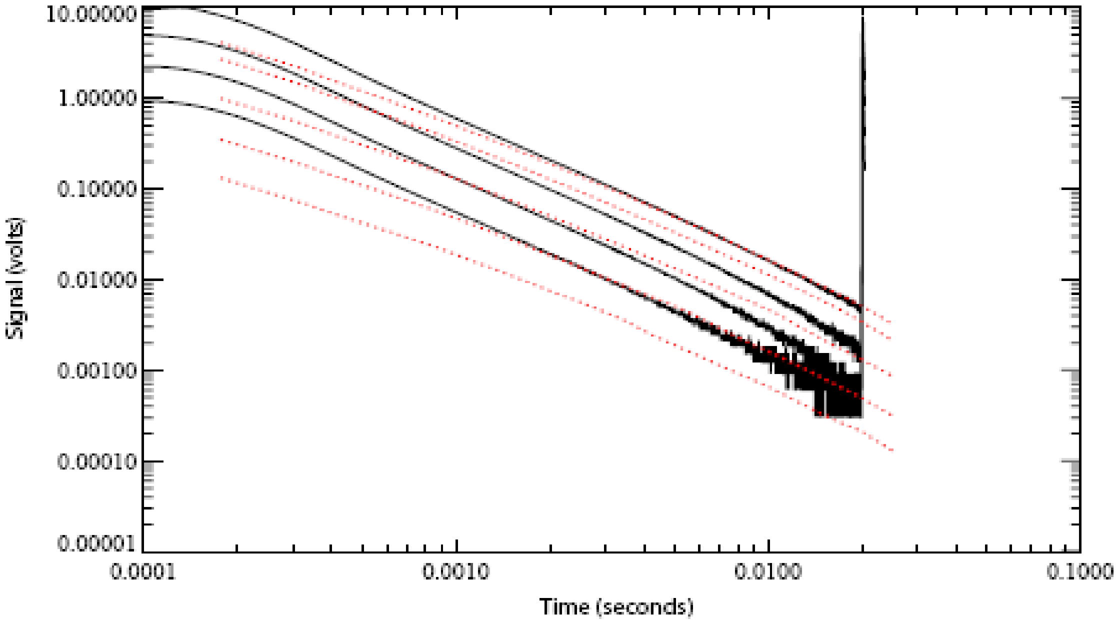

Figure 5.7b Black curves are responses of 4 inch steel sphere from our sensor using high gain INA103KP instrumentation amplifier in voltage measurement method at heights of 3, 6, 9 and 12 inches respectively and red dotted curves are from EM63 at heights of 2.5, 5, 10, 15 and 20 inches respectively (Log/Log).

It should be noted further that in case of the copper rings the responses are approximately straight lines on a log/linear plot while on a log/linear plot the sphere responses have an exponential shape. Thus the general shape of the response can be used to easily distinguish between ferrous and non ferrous objects.

5.2.2 Response of 1 by 4 inch and 2 by 8 inch steel cylinder

Figures 5.8 and 5.9 present data for a 1 by 4 inch steel cylinder when oriented with its axis perpendicular and parallel to the incident magnetic field. Figures 5.10 and 5.11 present similar data for a 2 by 8 inch steel cylinder.

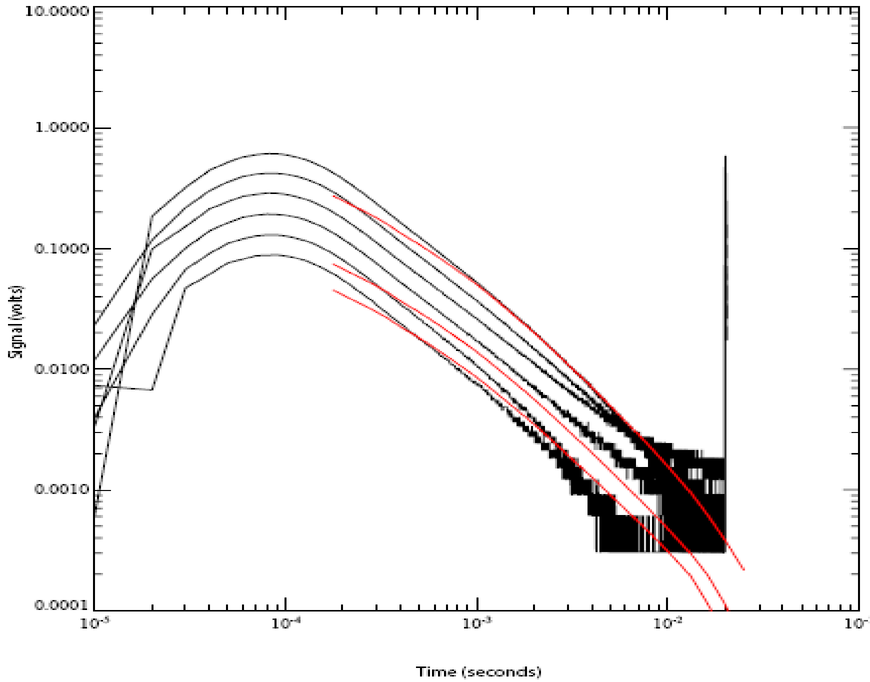

Figure 5.8 Black curves are responses of 1 by 4 inch cylinder in vertical positions at heights of 3,6,9,12 inches from our sensor using high gain INA103KP instrumentation amplifier in voltage measurement method and red curves are from the EM63 sensor at heights of 2.5,10 and 12.5 inches respectively (Log/Log).

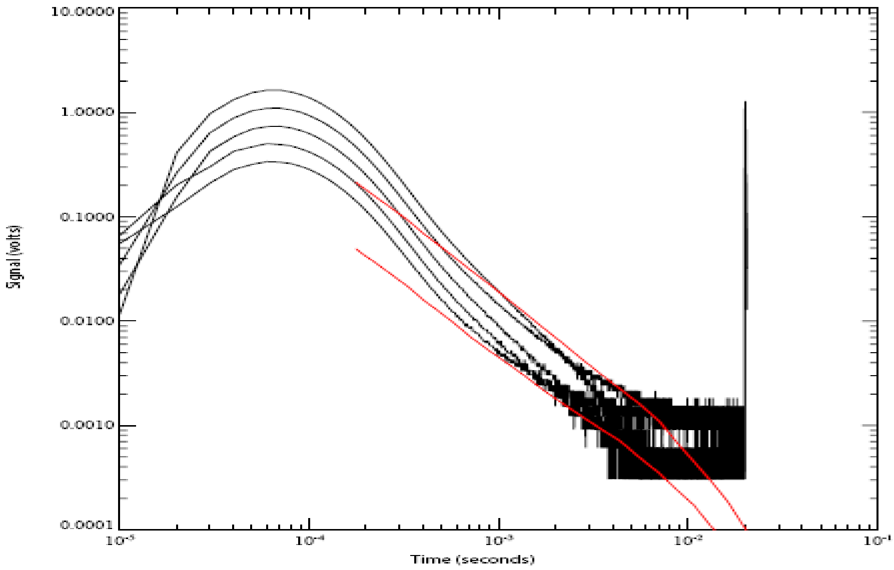

Figure 5.9 Black curves are responses of 1 by 4 inch cylinder in horizontal positions at heights of 3,6,9,12 inches from our sensor using the high gain INA103KP instrumentation amplifier in voltage measurement method and red curves are from EM63 sensor at heights of approximately 2.5 and 10 inches respectively (Log/Log).

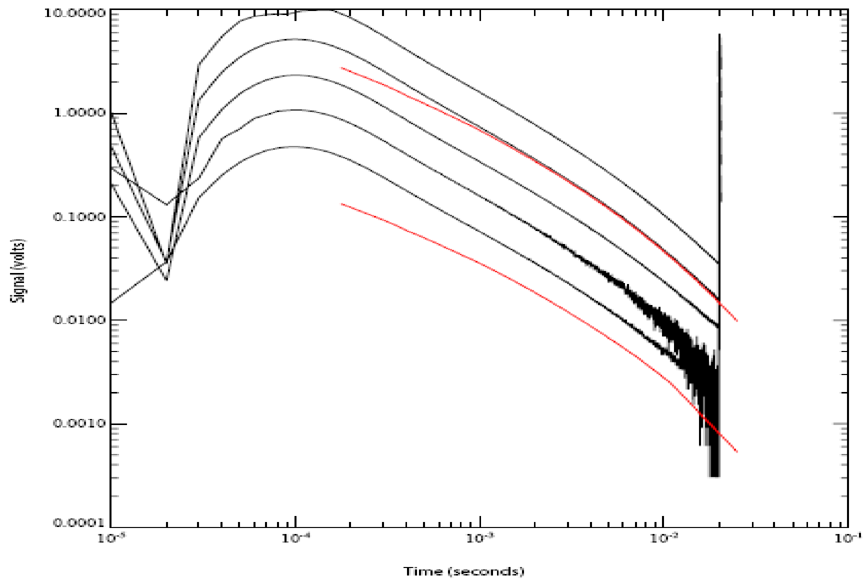

Figure 5.10 Black curves are responses of 2 by 8 inch steel cylinder in vertical positions at heights of 3,6,9,12 inches from our sensor using high gain INA103KP instrumentation amplifier in voltage measurement method and red curves are from EM63 sensor at heights of 10 and 25 inches respectively (Log/Log).

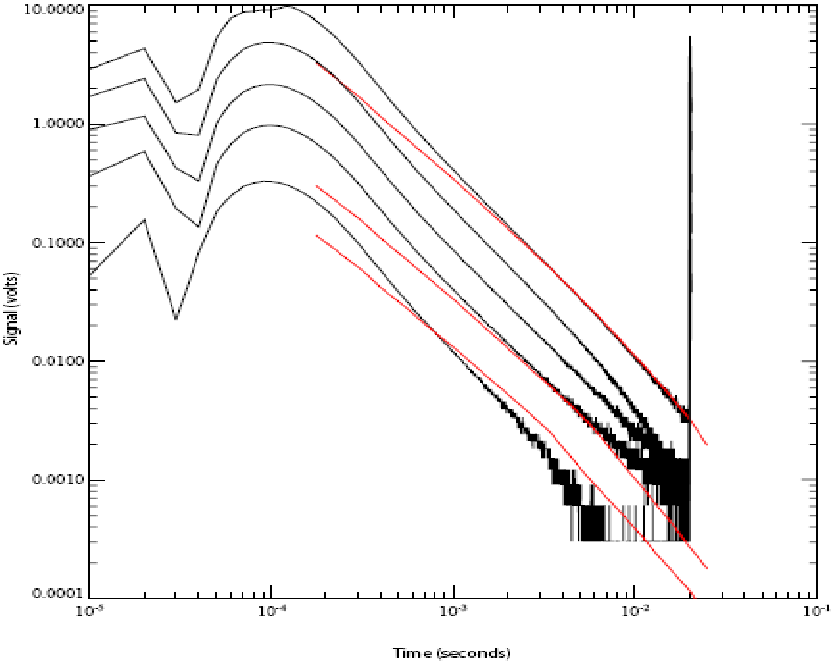

Figure 5.11 Black curves are responses of 2 by 8 inch steel cylinder in horizontal positions at heights of 3,6,9,12 inches from our sensor using high gain INA103KP instrumentation amplifier in voltage measurement method and red curves are from EM63 sensor at heights of approximately 2.5,15 and 20 inches respectively (Log/Log).

All target responses shown here are with background subtraction. Comparing the responses for different targets it can be observed that using a log versus linear scale yields a straight line response from the nonmagnetic copper rings while the response from ferrous targets like the steel sphere and cylinder are nonlinear on a log versus linear scale. However, when the ferrous targets are presented using a log versus log scale, an approximately linear response results. The performance from our sensor can be improved by using integration techniques to increase the signal to noise ratio especially in the late time when the signal strength is very weak. Also using a higher resolution A/D converter, minimizing noise from different sources including digitization noise, motion induced noise, location uncertainties, etc. can prove to be beneficial in enhancing overall sensor performance.

5.3 Summary

In this chapter the components used to construct our EMI time domain sensor were presented. Data collected with our sensor for various targets (ferrous and nonferrous) was compared with the same collected with the commercial sensor (the EM63). In the next chapter sensitivity plots for an arbitrary coil configuration are defined and a software tool is developed as a means of presenting sensitivity data in a graphical form. Sensitivity plots are particularly useful for developing a qualitative understanding of overall EMI system performance.

CHAPTER 6

SENSITIVITY AND STREAMLINE PLOTS FOR EMI SENSOR

This chapter introduces efforts made to develop and test a software tool for evaluating electromagnetic transmitter coil designs and configurations used in the geophysical detection of unexploded ordnance. The effort is directed towards developing a better understanding of the capabilities and limitations of Wide-Area Transmitter and Multi-Transmitter (WAT-MT) sensor systems.

6.1 Introduction

In order to evaluate EMI system performance in terms of sensitivity to different targets, static sensitivity maps can be used. Sensitivity maps provide a large amount of information about how effective a proposed coil layout can be [17]. Static sensitivity maps are a graphical representation that maps sensor response to a standardized infinitesimal object in a static field. These plots take in full account of both the transmitter and receiver coil shapes with no explicit consideration of target characteristics and are compact and are easy to understand.

6.1.1 Equations for static sensitivity

The static sensitivity $\sigma(P)$ of a set of coils is defined as the ratio of receiver coil flux linkage change to the flux linkages of the transmitter coil, per unit volume of the target in the limit of vanishing target size and is given as

$$\sigma(P) = \frac{3}{2}\frac{\mu_o}{L_{TT}}\frac{H_R \cdot H_T}{i_R i_T} \tag{6.1}$$

where σ (*P*) is static sensitivity at any space point P, $\mathbf{H}_R$ is the magnetic field at point P due to the receiver coil currents and $\mathbf{H}_T$ is the magnetic field at the same point due to the transmitter coil. Note that according to (6.1) the sensitivity is independent of transmitter and receiver currents because $\mathbf{H}_R$ and $\mathbf{H}_T$ are proportional to i_R and i_T, respectively. Therefore, sensitivity plots can be generated for a particular configuration of coils without reference to specific current values. In short, the aim of this graphical representation is to show the relative output change for an infinitesimal target when it is placed at different positions relative to the transmitter and receiver coils so that the uniformity and dynamic range of sensitivity can be assessed without reference to specific targets. The full derivation of (6.1) can be studied in [17]. Also we know that by Bio Savart's law the field at a point (P) in Figure 6.1 due to a straight current carrying conductor is given as

$$H = \frac{I}{4\pi\rho}(\cos\alpha 2 - \cos\alpha 1)a_\phi \tag{6.2}$$

Where, $\mathbf{a}_\Phi = \mathbf{a}_l \times \mathbf{a}_\rho$, ρ is perpendicular distance from conductor to point P and I is the current flowing in the conductor [18]. A computer program written using the latest release of Matlab (2006) has been developed using (6.1) and (6.2) for arbitrary configurations of transmitter and receiver coils to generate sensitivity maps. Appendix A provides more details about the software tool. The software allows the user to obtain sensitivity as well as streamline plots. Streamlines are useful when one is interested in visualizing the direction of the magnetic field due to the transmitter or receiver coil [19].

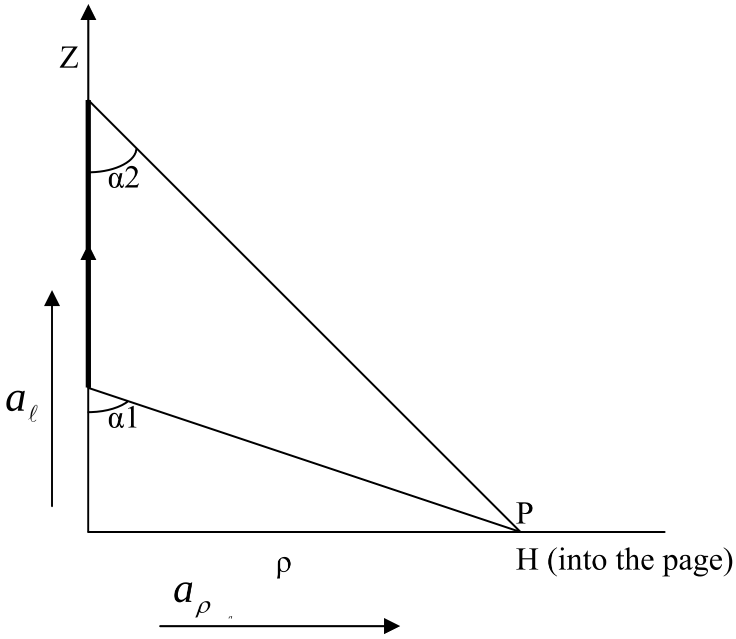

Figure 6.1 Conductor is shown as dark heavy line and the magnetic field due to it at P is into the page [18].

6.2 Sensitivity and streamline plots for different coil configuration

6.2.1 Simple configuration of two square coils

The first configuration considered is shown in Figure 6.2 and has been examined previously in [17]. It consists of two square symmetrically positioned coils with dimensions 984 mm (transmit coil) and 890 mm (receive coil). Figure 6.3a and 6.3b presents a contour plot of sensitivity on a plane parallel to the z-y plane extending from –60cm<z<-10cm and –80cm<y<80cm for x =0 and x=60cms. The contour plots reveal that there is a rapid decrease of sensitivity with depth and also a rapid change in the sensitivity pattern as distance along the x axis increases.

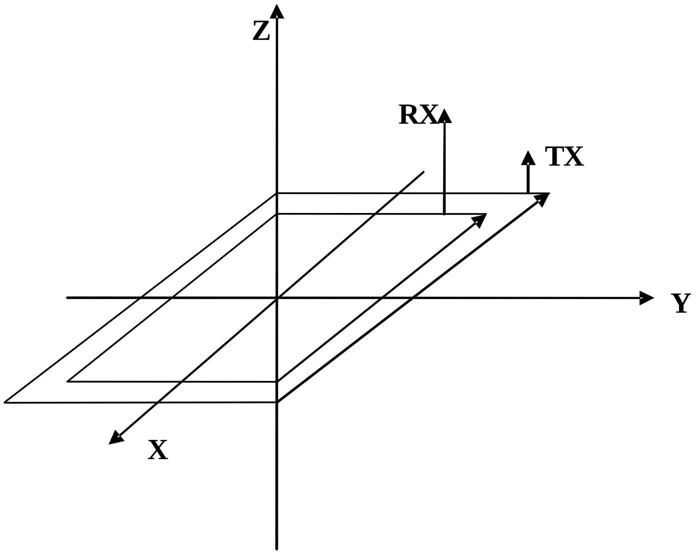

Figure 6.2 Square transmitter and receiver coils with dimensions 984 mm and 890 mm respectively. Current flows in counterclockwise direction in both the coils.

Figures 6.4a and 6.4b present sensitivity in dB along a line (linear plot) for z = 0 cm, and -150 cm < y < 150 cm for x= 0 and 60 cm respectively. From Figure 6.4a one can see that the sensitivity is maximum at the position of the conductors but further out (y>50 cm) it decreases rapidly. Also at the center the sensitivity is less than it is just above the conductors. But in Figure 6.4b at x=60 cm (further away from the plane of the coils) the sensitivity peaks at the center (y=0 cm) and then decreases monotonically on either side.

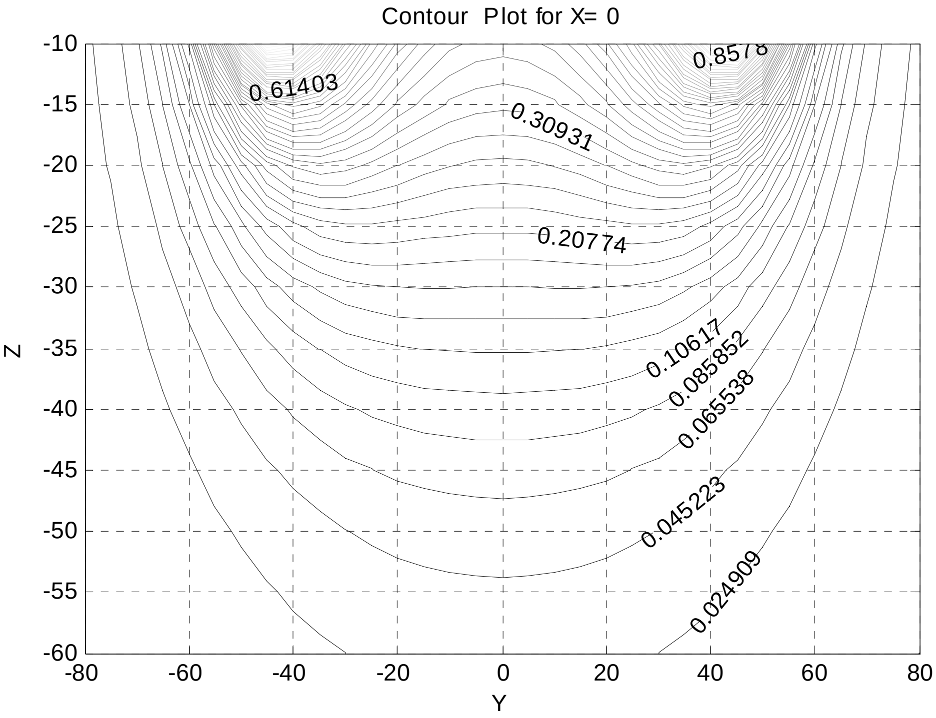

Figure 6.3a Sensitivity contours for coil configuration of Figure 6.2 computed over the plane x=0 cm, -80cm<y<80cm, -60cm<z<-10cm.

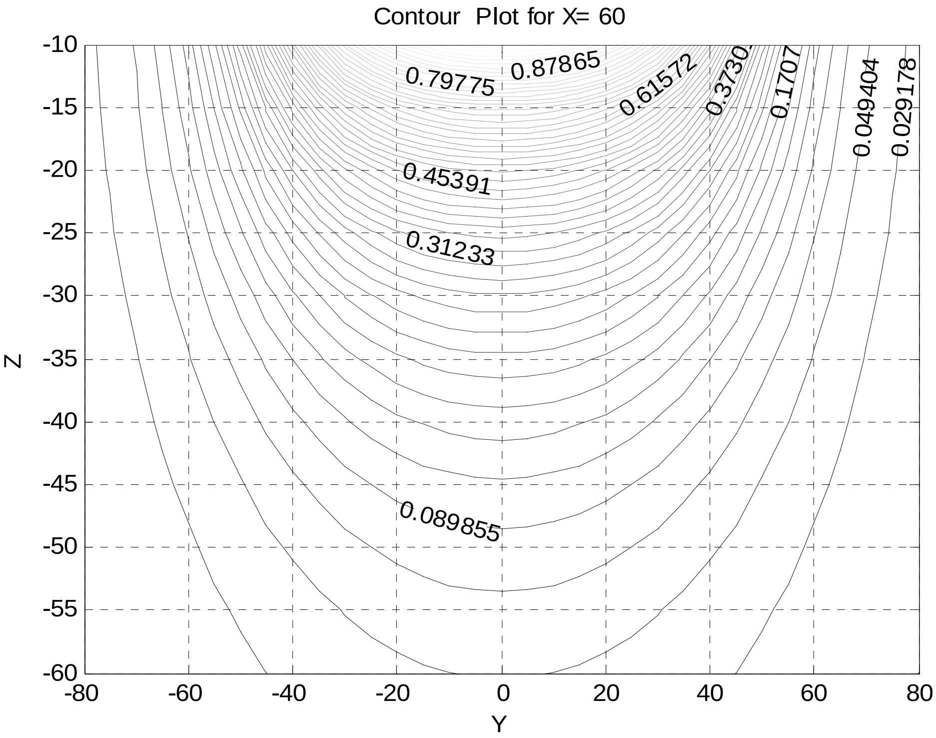

Figure 6.3b Sensitivity contours for coil configuration of Figure 6.2 computed over the plane x=60cm, -80cm<y<80cm, -60cm<z<-10cm.

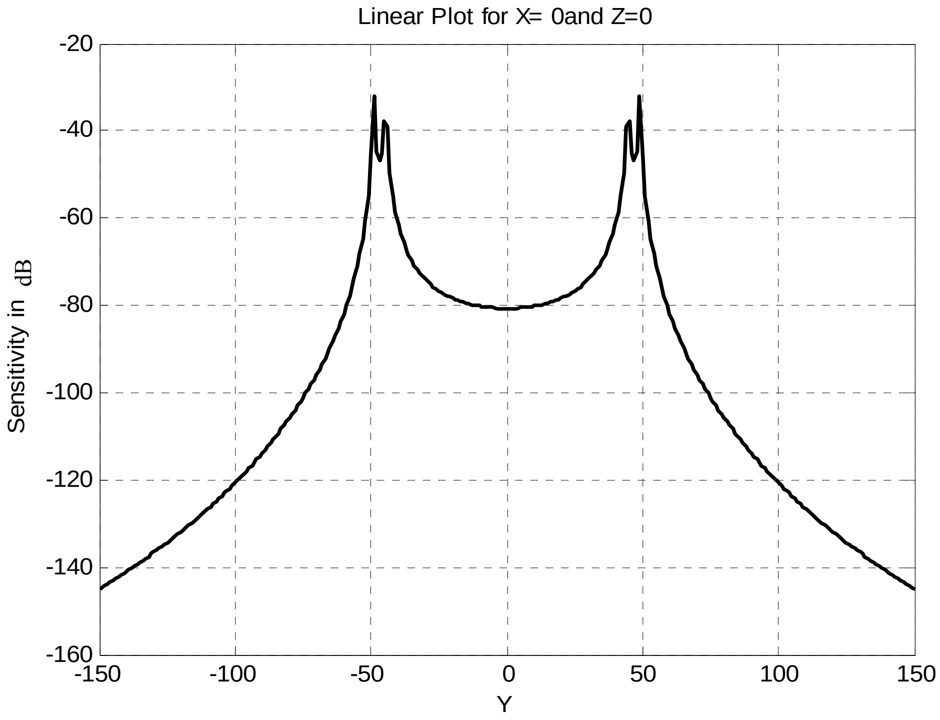

Figure 6.4a Sensitivity plot for coil configuration of Figure 6.2 computed along the line x= 0 cm, -150cm<y<150cm, z= 0 cm.

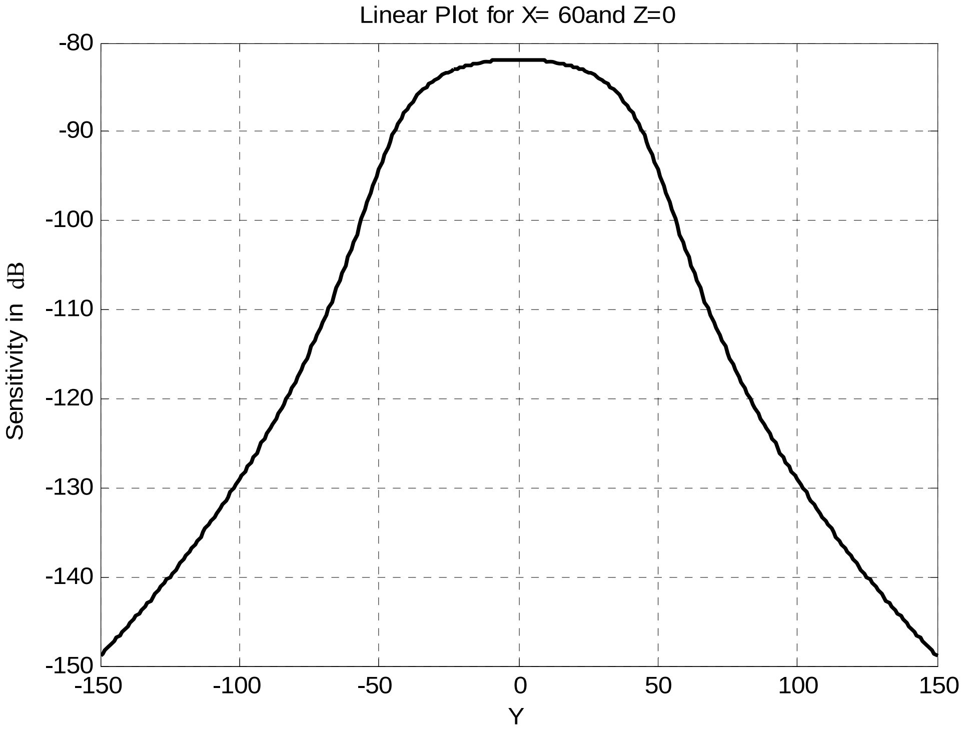

Figure 6.4b Sensitivity plot for coil configuration of Figure 6.2 computed along the line x= 60 cm,-150cm<y<150cm, z= 0 cm.

Figures 6.5 presents a color contour plot for the coil geometry in Figure 6.2 at a depth z=30 cm. In Figure 6.5 (in the plane of the coils) the most intense contours (colored red, yellow and light green) approximately trace out the location of the square transmitter and receiver coils. It was observed that as the depth increases the contours become elliptical and as expected the field gradient decreases. The relative peak values for contour plots can be easily determined by referring to their corresponding linear intensity plots as the values of sensitivity shown in contour figures are normalized and are in reference to that particular figure and not with respect to other figures.

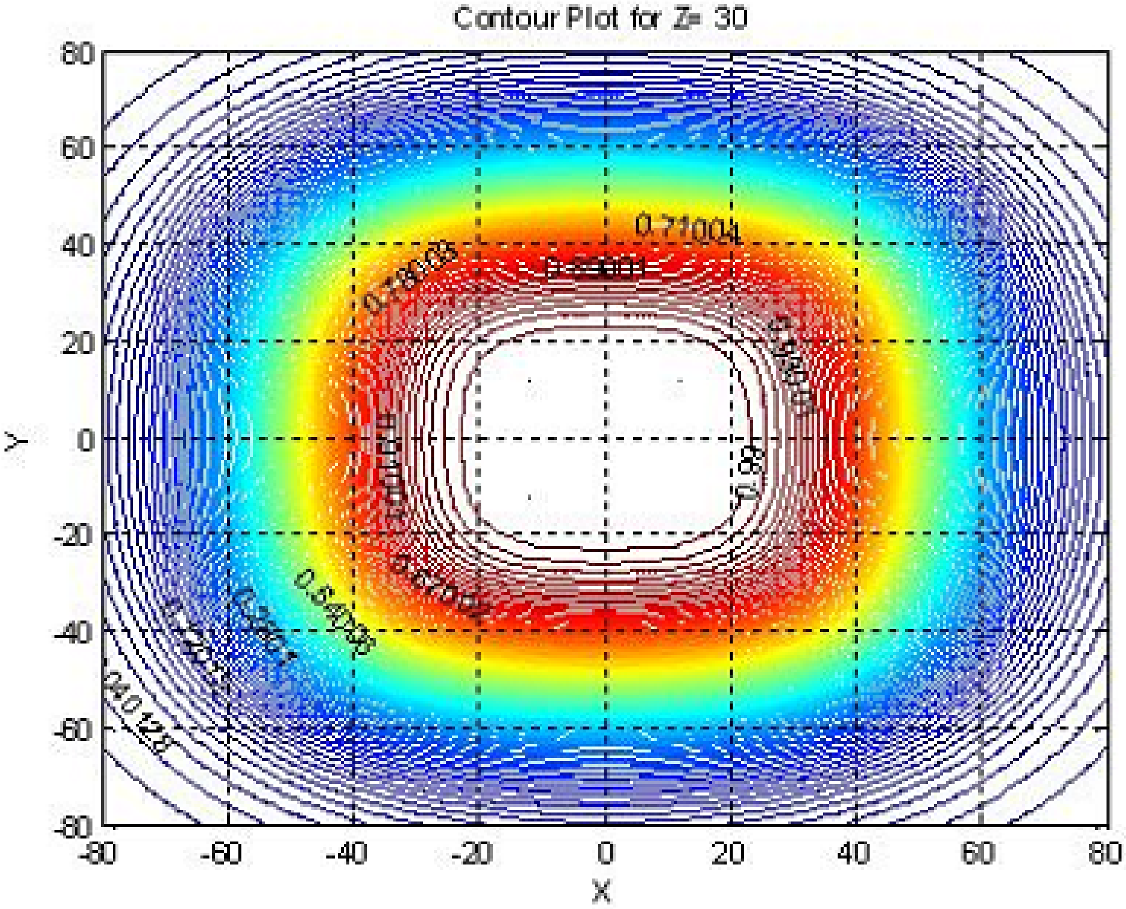

Figure 6.5 Color contour plot in the x-y plane at z=30 cm for the coil configuration of Figure 6.2.

Figure 6.6 shows the streamline plot for a simple 98.4 cm square coil (simple dipole) with current flowing in an counterclockwise direction (when observed from above). Since the plane of the plot cuts perpendicularly through the coils, the magnetic field forms closed loops near the conductors.

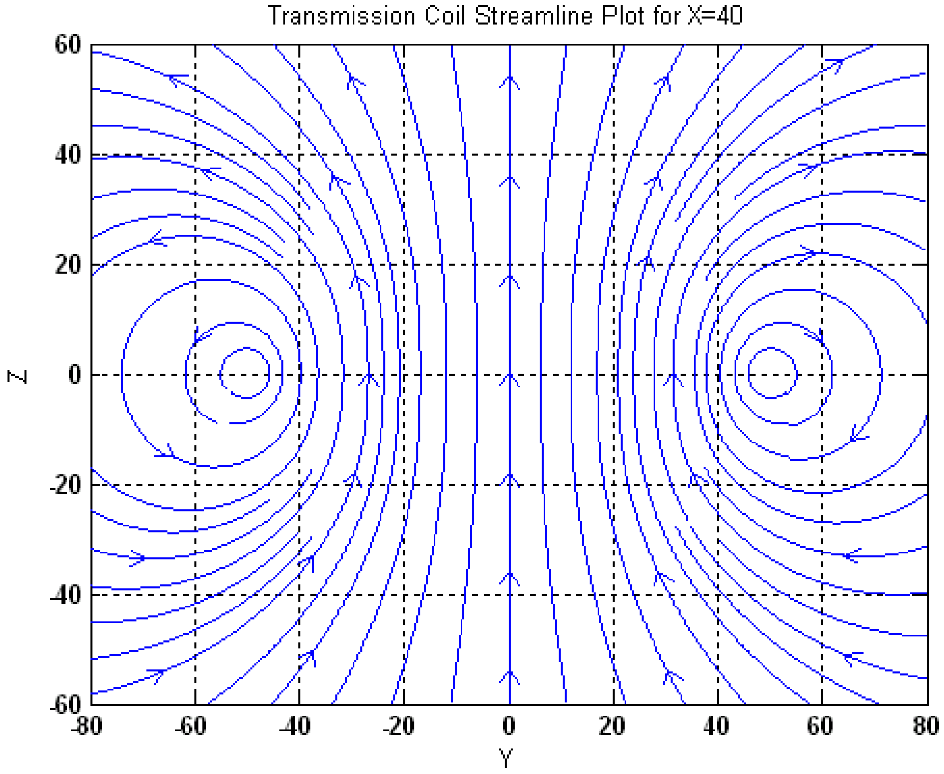

Figure 6.6 Streamline plot for 98.4 cm X 98.4 cm square coil centered in the x-y plane. Streamlines are computed for x = 40 cm and –80 < y < 80 cm, –60 < z < 60 cm.

6.2.2 Square transmitting coil and *figure 8* receiver coil

Figure 6.7 shows the next geometry of interest that consists of a square transmitter coil (identical to that shown in Figure 6.2) and a *figure-8* receiver coil. Note that according to the figure the currents on opposite halves of the receiver coil flow in opposite directions (counterclockwise in the +y coil looking down on the x-y plane from the positive z-axis and clockwise in the left hand –y coil). In contrast to this coil configuration, the configuration of Figure 6.2 has the disadvantage of large mutual coupling between detector and transmitter coils that may generate a voltage high enough to mask a weak target signal. The response when an object is positioned over the right receiver coil is of opposite polarity to that when the target is over the left side of the receiver coil and a null response occurs when the target is located anywhere on the symmetry plane (x-z plane). If this coil arrangement is moved in the direction of the y-axis a plus-zero-minus target response will be recorded. Of course, one obvious disadvantage of this coil arrangement is that if the coils move in the x-direction any target along the symmetry plane (x-z plane) will go undetected. It may be said that this coil arrangement has a *blind spot*. Another disadvantage of this so-called quadrupole receiver coil is that its sensitivity is, generally speaking, less than that of a standard dipole receiver coil with the same total area. The reason for the reduced sensitivity can be easily explained. Suppose the target's x and y-position is fixed so as to place the target at the middle of one half of the receiver coil. If the target is next moved along a line parallel to the z-axis (directly away from the plane of the coils) the response from each receiver coil begins to cancel since the difference in the distance between the target and the center of each half of the receiver coil approaches zero. So in general, the advantages of the quadrupole receiver over that of the standard dipole receiver coil come at the expense of reduced sensitivity.

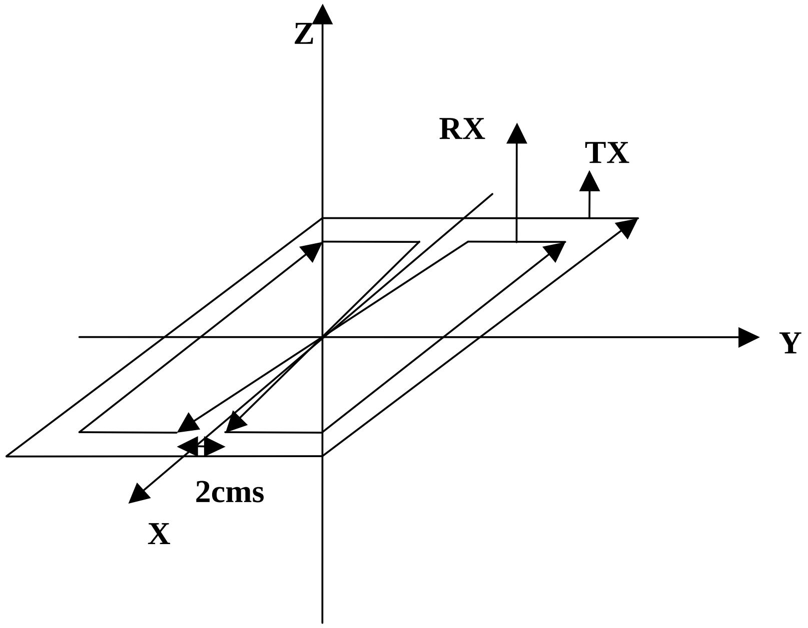

Figure 6.7 Square transmitter coil 984 mm on a side and *Figure-8* receiver coil – each half 44.5 cm X 89 cm. This coil has a blind spot (zero response) when the target is located anywhere in the x-z plane.

Figure 6.8 provides sensitivity contour plot in the y-z plane at x=0 cm. Note that the sensitivity everywhere on the y=0 plane (plane of symmetry) is zero. Peak sensitivity occurs near the coils and rapid field gradients exists along the z = -10 cm line in Figure 6.8. Figures 6.9a, 6.9b are plots of sensitivity along the y-axis (Figure 6.9a) and along lines parallel to the y-axis at x= 60 cm (Figure 6.9b). Close in, the sensitivity peaks near the coils at y = ± 50 cm and just to the left and right of the origin (Figure 6.9a). However, at x= 60 cm (Figure 6.9b) (outside the coils) the sensitivity peaks at y-values corresponding approximately to the center of the receiver coils. Figure 6.10 provide sensitivity contour plots in plane parallel to the x-y plane, but below the plane of the coils, at z = -30 cm. It can be seen that the most intense sensitivity contour lines (red, yellow and green) occupy a large area of the plot indicating that sensitivity falls off slowly (low field gradient) relative to what would occur in a plane close to the coils.

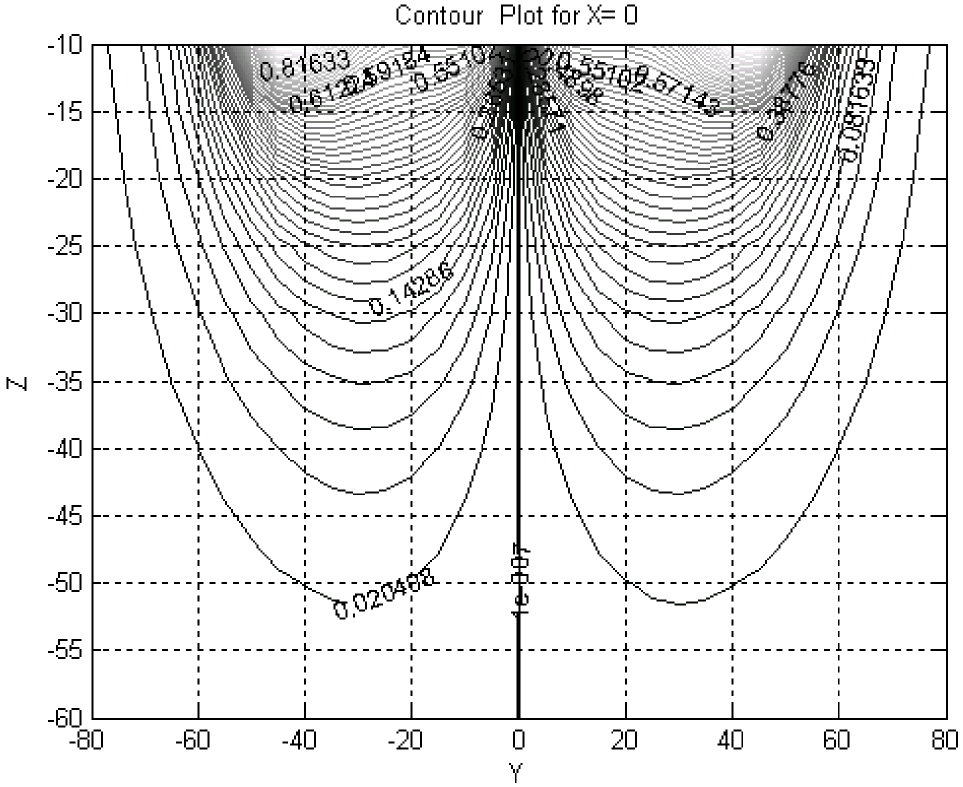

Figure 6.8 Contour plot of sensitivity for the *figure-8* receiver coil configuration of Figure 6.7. Plot is given for –10 cm < z < -60 cm and –80 cm < y < 80 cm at x = 0 cm.

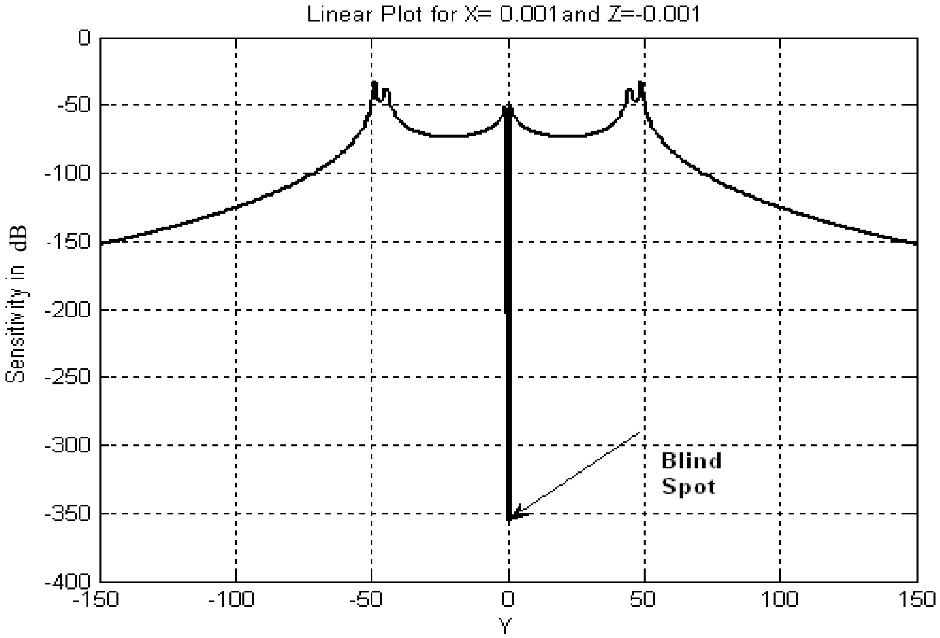

Figure 6.9a Linear plot of sensitivity for the *figure-8* receiver coil configuration of Figure 6.7. Plot is given for –150 cm < y < 150 cm at x = z = 0 cm.

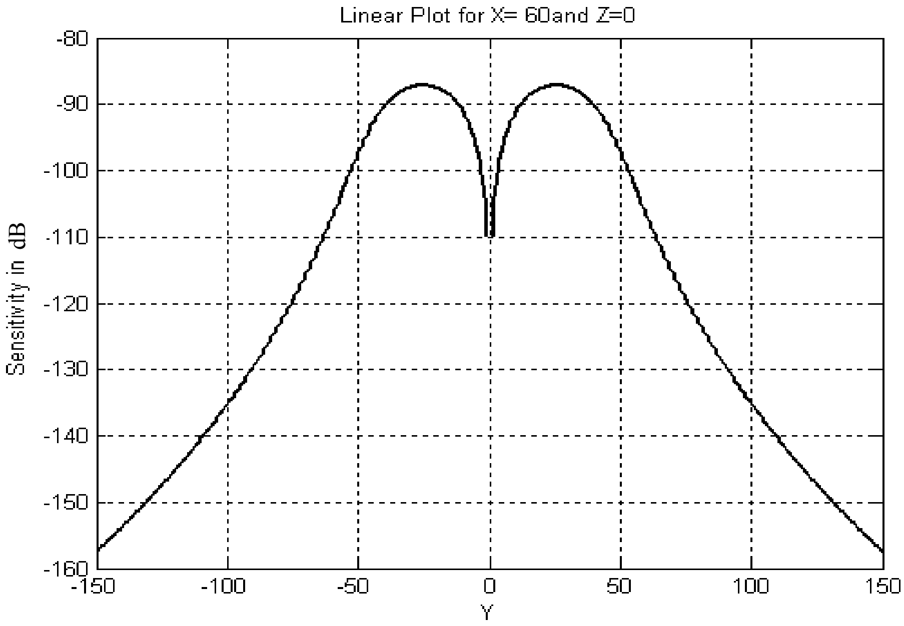

Figure 6.9b Linear plot of sensitivity for the *figure-8* receiver coil configuration of Figure 6.7. Plot is given for –150 cm < y < 150 cm at x = 60 cm and z = 0 cm.

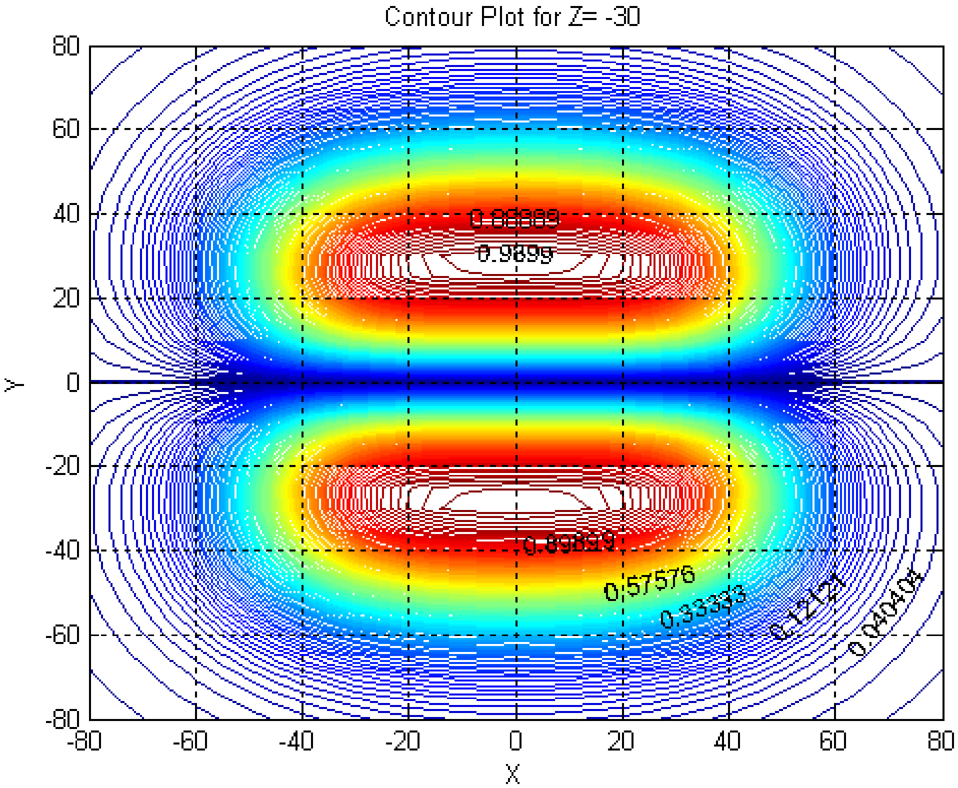

Figure 6.10 Contour plot of sensitivity for the *figure-8* receiver coil configuration of Figure7. Plot is given in the plane parallel to but beneath the coils; z= 30 cm -80 cm < y < 80 cm and –80 cm < x < 80 cm.

6.2.3 Stacked arrangement of three square coils

Shown in Figure 6.11 is a stacked arrangement of three 1m X 1m coils with 50 cm spacing. The middle coil is the transmitting coil placed in the xy plane at z=0cms and the upper and lower coils are receiving coils placed in xy plane at z=+50cms and z=-50cms respectively and are assumed to have oppositely directed currents.

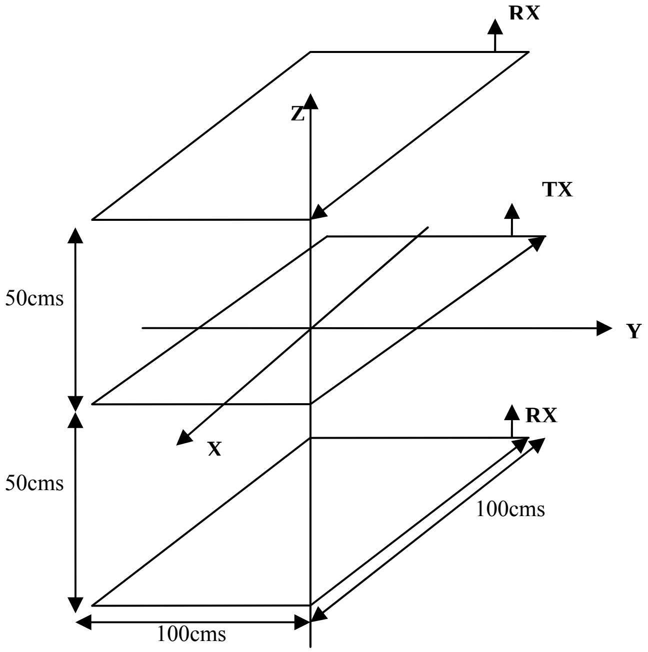

Figure 6.11 A stacked arrangement of three 100 cm square coils. The center coil is the transmitter at z=0cms and the upper and lower coils are receivers at z=+50cms and z=-50cms respectively. Currents in the receiver coils flow in opposite directions.

Figure 6.12 shows how the sensitivity along the z-axis changes as the distance between transmitter and each receiver coil decreases from 50 cm to 10 cm. Note that the 50 cm spacing results in a sensitivity increase of approximately 15 dB over that achieved with the 10 cm spacing. Of course in the limit of zero spacing between receiver coils the sensitivity would be everywhere zero. The sensitivity when the receiver coils are separated by 1 m is significantly greater (approximately 20 dB) then when the coils are only separated by 20 cm.

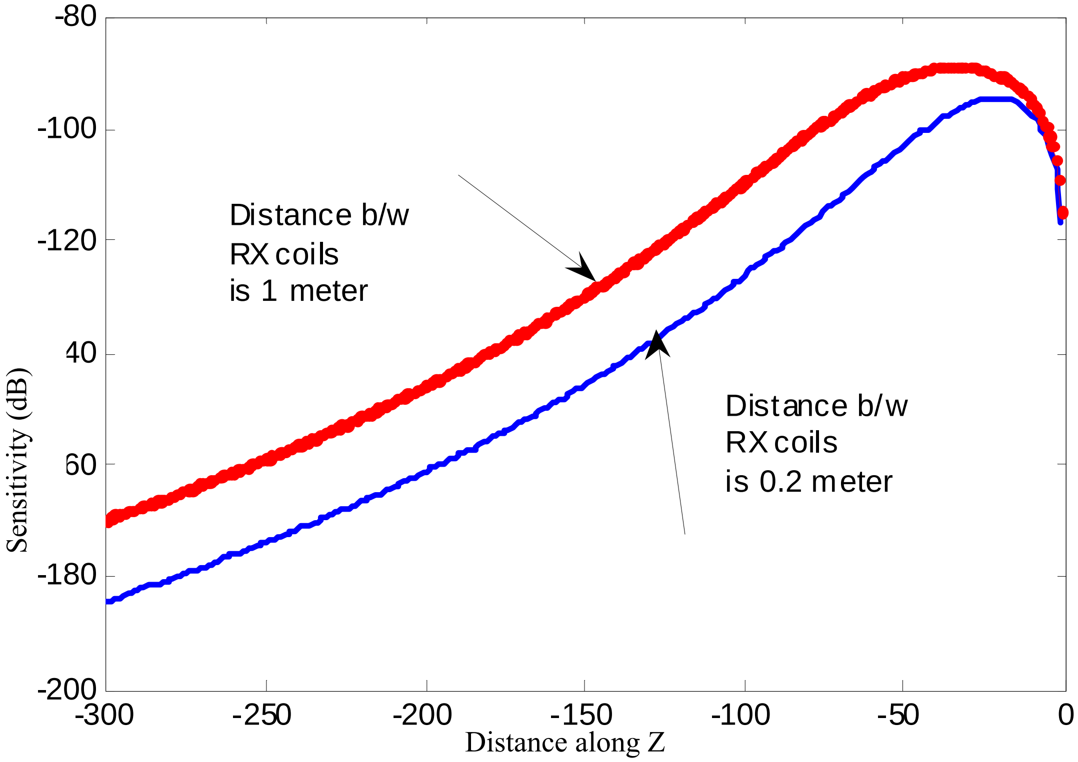

Figure 6.12 Linear plot of sensitivity in dB along the z-axis for –300 cm <z< 0 cm versus distance along z axis. The red curve is for the stacked configuration of Figure 6.11 while the blue curve is for an identical geometry to that of Figure 6.11 except that the distance between receiver coils is reduced from 100 cm to 20 cm.

6.2.4 Two square transmitter and two square receiver coils in same plane (XY plane)

Figure 6.13 shows two transmitters 1m by 1m separated by a distance d and two receivers 0.5m by 0.5m and placed symmetrically inside transmitter coils. All coils are in phase with current flowing in an counterclockwise direction. Figure 6.14 shows an interesting sensitivity plot for this configuration along z axis. The figure is counterintuitive from the point of view that sensitivity decreases with distance along the z axis, reaches a null (very low) value and then increases again as distance increases.

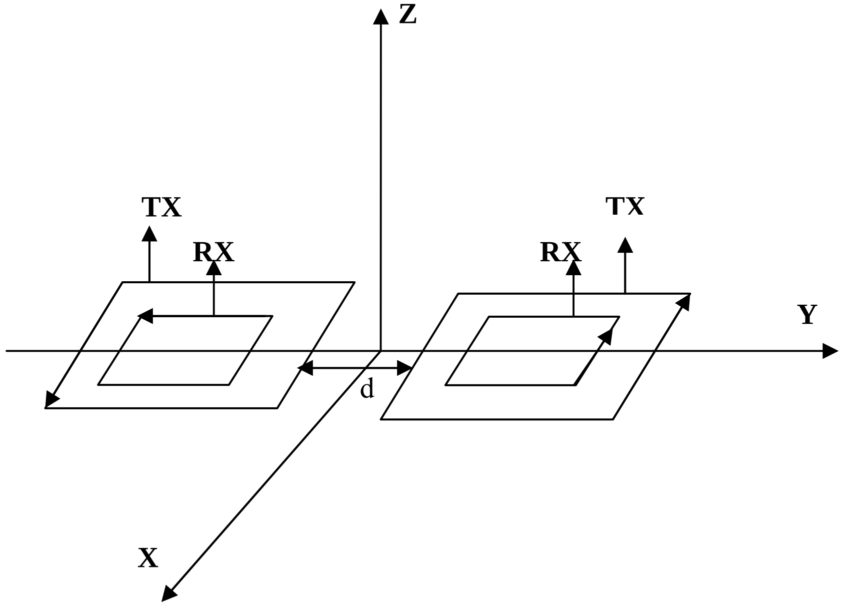

Figure 6.13 Coplanar configuration showing two transmitters (TX) 1m by 1m and two receivers (RX) 0.5m by 0.5m with current flowing in all the coils in counterclockwise direction.

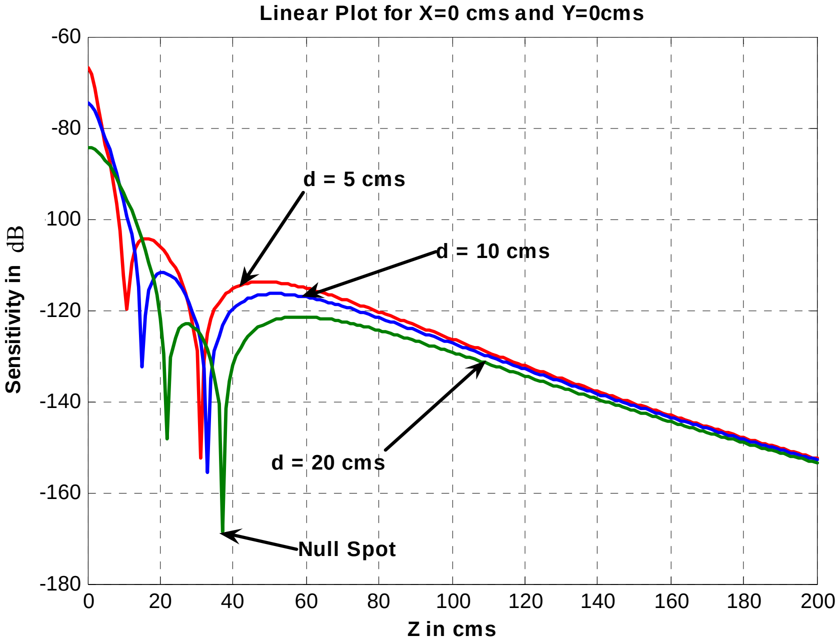

Figure 6.14 Linear plot of sensitivity in dB versus distance along z axis for configuration shown in Figure 6.13. There is a null at some point and then sensitivity starts increasing again with distance.

6.3 Comparison of measured to calculated sensitivity plot for the Geonics EM-63

In this section measured and calculated sensitivity plots for a pulsed electromagnetic induction sensors, the EM-63, manufactured by Geonics Ltd [12] are compared. Figure 6.15 shows the EM-63 coil arrangement and experimental setup.

Figure 6.15 EM-63 coil arrangement and experimental Setup.

As shown in Figure 6.15 the bottom large coil is 1m X 1m and symmetrically located within the boundary of the transmitter coil are two 21 inch X 21 inch receiver coils. The lower coil is in the same plane as the transmitter coil while the upper coil is 12 inches above the plane of the transmitter coil. The gray cinder blocks support a 4 ft. X 8 ft. sheet of peg board with an x-y grid of 1 inch spaced holes. The edge of the peg board (nearest the observer) runs along the centerline of the coils 17 inches above the transmitter coil. Data was collected by moving a 2-inch x 8-inch ferrous cylinder across the centerline of the coil arrangement in 2-inch increments.

Ordinarily, the EM-63 has a third coil attached 12 inches above the middle coil resulting in a three-receiver coil arrangement. In this experiment the upper coil was removed and the wires that would ordinarily connect this coil to the EM-63 preamplifier were shorted. The measured response therefore is due *only* to interaction between the transmitter coil, lower receiver coil, and 2 inch X 8 inch vertical cylinder. Figure 6.16 shows the voltage corresponding to the first time gate of the EM-63 as a function of position of the 2 inch X 8 inch cylinder as it is scanned over the top of the coils. The corresponding sensitivity plot is shown in Figure 6.17 and one observes reasonably good qualitative agreement between measurement and predictions although a more careful comparison between measurements and predictions is planned for the near future.

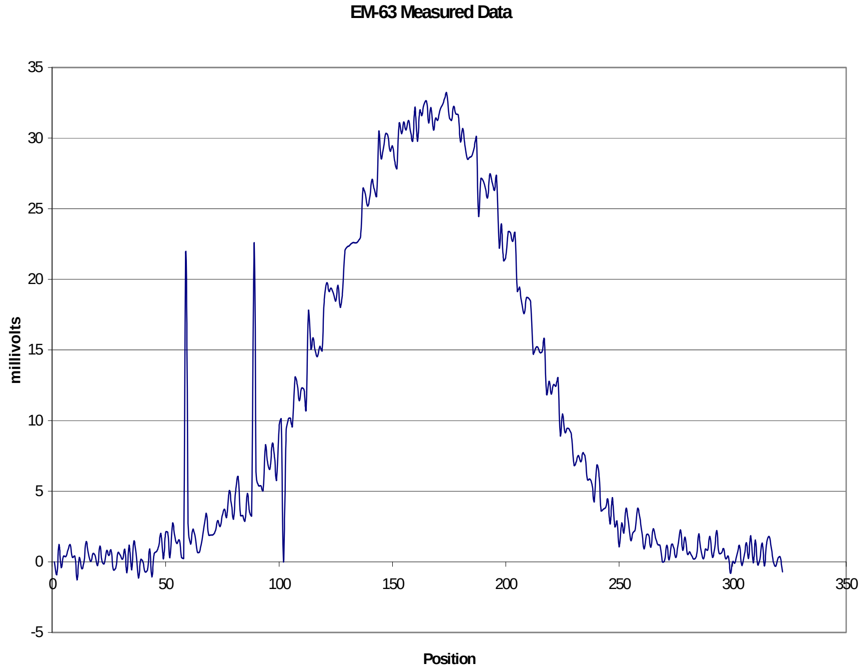

Figure 6.16 Measured response from EM-63 due to a 2 inch X 8 inch ferrous cylinder. The response is determined by plotting the voltage induced in the lower receiver coil corresponding to the first time gate of the EM-63 [13].

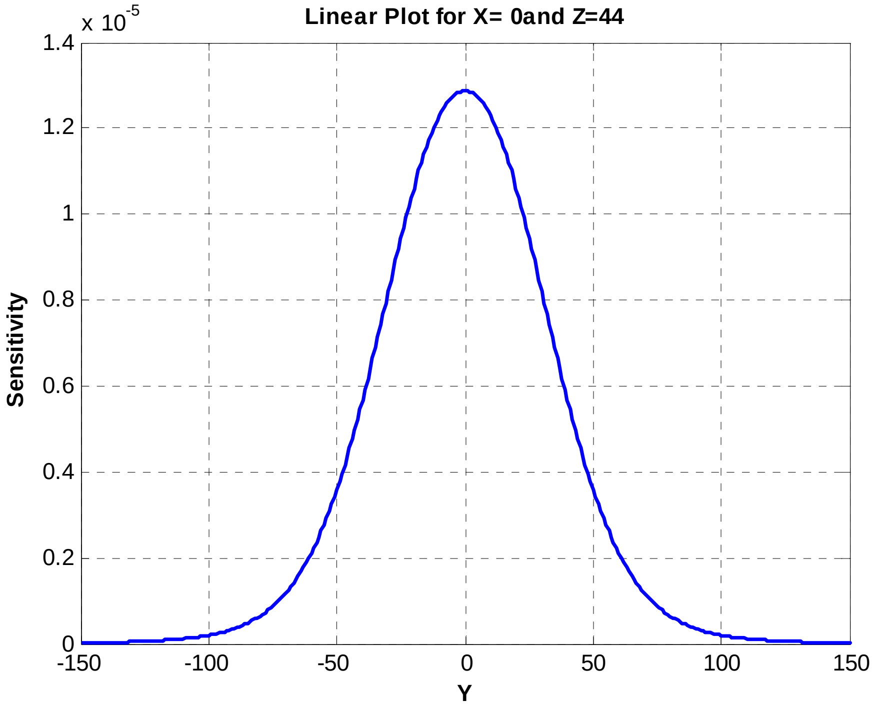

Figure 6.17.Sensitivity for a coil configuration consisting of a 1m X 1m transmitter coil and a symmetrically located 21 inch X 21 inch coplanar receiver coil. Sensitivity is computed along the centerline 17 inches above the coils.

6.4 Summary

In this chapter a simple method has been presented to compare the sensitivity of different candidate coil designs used for the purpose of detecting unexploded ordinance (UXO). Sensitivity is proportional to the dot product of the transmitter and receiver coil magnetic fields assuming each coil supports unity current. Sensitivity is determined over a planar grid of points parallel to one of the Cartesian coordinate planes or along a line parallel to one of the Cartesian axes. Additionally, streamline plots provide a method of visualizing the direction of the magnetic field produced by a candidate coil design. Several different coil configurations have been investigated using the Matlab program described in the Appendix A. A square-transmitter coil with square-receiver coil design was compared to a design consisting of a square-transmitter coil and figure-eight receiver coil design. Although the figure eight design has less sensitivity than the square coil design it has the advantage of marking more precisely the location of the target since the response passes through a null as the target moves from one half of the figure eight coil to the other. Good qualitative agreement was observed when sensitivity measurements were compared with calculations for the EM-63 manufactured by Geonics Ltd [13].

CHAPTER 7

CONCLUSION

This thesis presents efforts towards improving the detection and discrimination capability of a Time-Domain (Pulsed) EMI system. Several lab experiments have been performed to test the performance of EMI systems and wherever possible analytical explanations have been provided to improve overall understanding of the performance observed. Chapters 2 and 3 provide an overview of basic concepts of an EMI system and also explain several issues that should be considered while designing hardware for both voltage and current measurement methods. In chapter 5, the measurements from our TD sensor and the EM63 sensor have been compared and lastly, in chapter 6 Electromagnetic Induction (EMI) coil sensitivity maps for evaluating coil designs and configurations used in the geophysical detection of unexploded ordnance have been described.

We are currently planning to make sensitivity measurements with a collinear (side-by-side) array of EM-61 coils. Of particular interest is the response of a target as it is moved perpendicularly away from but between the coils. For this case, the linear sensitivity plot had an interesting but unexpected feature. Namely, the sensitivity begins to decrease with increasing target distance (as expected) but then a null position is reached and finally as the distance continues to increase then increases back to the value just before the null. Therefore a *blind spot* was observed between even closely spaced coils. This blind spot was indeed observed in measurements made with three side-by-side EM-61 coils. However, two out of the three EM-61 systems used were not functioning properly and have been returned to Geonics for repair. We intend to revisit this interesting phenomenon as soon as the defective systems are repaired. We also intend to modify our sensor circuitry further by putting integrators to boost the late time object response which is very weak.

BIBLIOGRAPHY

[1] Article on unexploded ordnance in Wikipedia, an online encyclopedia, available online at http://en.wikipedia.org/wiki/Unexploded_ordnance

[2] "Landmine Monitor Report 2006," available online at: www.icbl.org

[3] Eugene Lavely, Robert Grimm, and Peter Weichman, "Detection and Discrimination of UXO", available online at https://www.denix.osd.mil/denix/Public/News/OSD/UXO/Conferences/Forum/Lavely.pdf

[4] J.N. Palasagaram, *Efforts towards the design and development of an electromagnetic induction sensor optimized for detection and discrimination of unexploded ordnance*, Master's Thesis, Auburn University, 2006

[5] K.B.Loyd, *Design and construction of a pulsed electromagnetic induction system for unexploded ordnance detection and discrimination*, Master's Thesis: Auburn University, 2004.

[6] F. S. Grant and G.F. West, *Interpretation Theory in Applied Geophysics*, New York: McGraw-Hill Book Company, 1965.

[7] C. E. Baum, *Detection and Identification of Visually Obscured Targets*, Taylor and Francis, 1999 (Chapter 6).

[8] Claudio Bruschini, A multidisciplinary analysis of frequency domain metal detectors for humanitarian demining, Doctoral's Thesis, Vrije Universiteit Brussel, 2002

[9] C.A. Balanis, *Advanced Engineering Electomagnetics*. New York: John Wiley & Sons, Inc, 1989

[10] L.S. Riggs, "EMI Sensor Optimized for UXO Discrimination-Annual Report," *Auburn University*, January 2005

[11] R.J. Prance, T.D. Clark, H. Prance, "Compact broadband gradiometric induction magnetometer system," *Sensors and Actuators*, Vol 76 (1999), pp. 117-121.

[12] "EM63 Catalogue," available online at: www.geonics.com

[13] “EM63 Full Time Domain Electromagnetic UXO detector Operating Instructions,” May 2003, available at http://www.geonics.com

[14] Datasheet of LT1028 – Ultra low noise precision high speed op amps, available online at http://www.linear.com/pc/downloadDocument.do?navId=H0,C1,C1154, C1009,C1026,P1234,D3480

[15] Datasheet of MAX 430- ± 15V chopper stabilized operational amplifier, available online at http://datasheets.maxim-ic.com/en/ds/MAX430-MAX432.pdf

[16] Information on Compuscope 1602, high speed digitizer, available online at http://www.gage-applied.com/Products/digitizer_pci/16_bit/compuScope_1602.htm

[17] P. S. Silvester and D. Omeragic, “Sensitivity Maps for Metal Detector Design,” IEEE Transactions on Geosciences and Remote Sensing, 1996

[18] Matthew N.O Sadiku, *Elements of Electromagnetics,* Third Edition, Oxford University Press, Inc

[19] S. M. Wentworth, *Fundamentals of Electromagnetics with Engineering Applications*, John Wiley and Sons.

[20] P. Kašpar, P. Ripka, “Induction Coils: voltage versus current output,” *Imeko World Congress*, Vienna 2000, Vol. V, pp. 55-60.

[21] L.S. Riggs, “EMI Sensor Optimized for UXO Discrimination-Annual Report,” *Auburn University*, January 2005

[22] N. Jain, L.S. Riggs, Bob Selfridge, “Electromagnetic Induction Coil Sensitivity Maps for Evaluating Coil Designs and Configurations Used in the Geophysical Detection of Unexploded Ordnance ,” SAGEEP Conference Paper, 2007

APPENDIX A

A.1 Using the software tool

Matlab was used to create a GUI that will enable the user to enter a geometry file that contains information defining the transmitter and receiver coils corresponding to a particular sensor. Sensitivity plots are generated with the press of a button and either linear plots or contour plots, in any plane defined by the user can be generated. Of course the user has to specify the range for each of the coordinate axes and also the coordinate value where the computation plane is located (e.g scan over x and y with z fixed or scan over y and z with x fixed, etc.). The interface for streamline plots is very similar to that for sensitivity plots with only a minor change in the computational engine.

A.2 Explanation of the Code

Each sensor coil is treated as a set of straight conductors with start and end points and equation (6.2) has been used to calculate the magnetic field due to that conductor at any given point on the observation plane. The total magnetic field due to a coil is thus calculated by adding the magnetic field due to each segment which makes up the coil. This method enables one to calculate the total magnetic field due to the transmitter configuration, which, in general may consists of several coils. A similar method is followed to calculate the total magnetic field due to the receiver unit which may also consist of a large number of coils. Thus in the geometry file the user enters information about the total number of straight conductors in the transmitter and receiver units respectively and the start and end points of each one of them. Using equation (6.2) the dot product of the total magnetic fields due to both the units is taken and is plotted as linear or contour plot. The current flowing in the transmitter and receiver coils is assumed unity as sensitivity is independent of currents according to equation (6.1). The components of magnetic field have units (Amp/K) where K can be meters, millimeters or centimeters depending upon the values that user inputs in the geometric file for his sensor. All the plots in this report were generated using centimeters. For streamline plots of transmitter coil fields the total magnetic field due to the transmitter was calculated as discussed above and the Matlab *streamslice* command was used to plot the corresponding data.

A.3 Limitations of the code

1) User has to enter geometric file that can be a significant work for sensors having large number of coils. An alternative method might be explored to improve data entry.

2) Some sections of the code use *for* loops that slow execution times especially for large sensor configurations. Some effort was expended to avoid using *for* loops but this resulted in an unexpectedly large data array which again resulted in lengthy run time.

3) The user may run into cases where a generated plot doesn't make much sense which may occur for instance when the distance between the space point and the coil is zero or the range of the space coordinates is too large for the *for* loop to execute. In such cases changing space coordinates usually resolves the problem.